Electronic Research Archive

http://www.aimspress.com/journal/era

ERA, 34(2): 694–722.
DOI: 10.3934/era.2026032
Received: 26 September 2025
Revised: 25 December 2025
Accepted: 09 January 2026
Published: 22 January 2026

Research article

Fractional variable transformation neural networks for analytical solution of nonlinear fractional partial differential equations

Limei Yan[1,‡], Shanhao Yuan[1,2,‡], Yanqin Liu[1,*], Runfa Zhang[3,*] and Qiuping Li[1]

[1] School of Mathematics and Big Data, Dezhou University, Dezhou 253023, China

[2] School of Mathematics and Statistics, Qilu University of Technology (Shandong Academy of Sciences), Jinan 250353, China

[3] School of Automation and Software Engineering, Shanxi University, Taiyuan 030013, China

‡ The authors contributed equally to this work.

* **Correspondence:** Email: yqliumath@163.com, rf_zhang@sina.cn.

Abstract: In this paper, we propose fractional variable transformation neural networks (fVTNNs, for short), a framework that embeds fractional variable transformation into neural networks (NNs), to systematically derive analytical solutions for nonlinear space-time fractional partial differential equations (fPDEs) via symbolic computation. This approach significantly enhances both the computational speed and the result precision by combining the robust approximation capacity of NNs with the exactness of symbolic computation. The output of fVTNNs, which consists of weights, biases, and activation functions, is taken as a trial function for the considered equation. In order to explain the feasibility of the proposed method, some examples are investigated. Hyperbolic function solutions and exponential function interactive solutions of these equations are obtained. The analytical solutions obtained using this method are accurate and have no calculation errors. To visualize the dynamic characteristics of the solutions, three-dimensional plots, contour plots, and density plots are employed. This research introduces a novel computational framework for obtaining exact solutions to fPDEs, with a broad applicability in science and engineering.

Keywords: neural networks; symbolic computation; nonlinear fractional partial differential equations; fractional Burgers-type equation; exact solution

1. Introduction

Fractional calculus has been shown to be applicable in a variety of subjects, including fluid mechanics, biology, medicine, engineering, and other scientific domains [1–5]. In recent decades,

fractional order partial differential equations (fPDEs) have become a highly studied topic in mathematics and physics [6–8]. Because of the widespread use of these equations, many well-known mathematical and physical equations with integer-order derivatives have been generalized to fractional counterparts, such as fractional heat conduction equations, fractional Schrödinger-like equations, fractional diffusion equations, fractional Burgers equations, etc [9–12].

Nonlinear phenomena play an important role in applied mathematics, physics, mechanics, and biology. Therefore, the explicit solutions of nonlinear fPDEs are crucial to maintain the physical properties of the problem and to thoroughly understand the described process. Nonlinear fPDE solutions have become a study priority in order to better investigate the underlying complicated physical phenomena and apply them to real-world applications. Many effective methods have been developed to construct analytical or approximate solutions for nonlinear fPDEs, including the finite difference method [13–15], finite element method [16–18], spectral method [19–22], fractional homotopy perturbation method [23–25], $(\frac{G'}{G})$-expansion method [26–28], Lie symmetry analysis [29–32], and so on.

However, to our knowledge, most of the solutions obtained by the above mentioned approaches were either numerical or approximate, and methods for finding analytical solutions to fPDEs have received relatively little attention so far. As El-Sayed [33] pointed out, there is some difficulty in finding analytical solutions for fPDEs, which are becoming more common in numerous academic domains and engineering applications. To solve such equations, an efficient and user-friendly approach is required.

With the advancement of artificial intelligence, deep learning methods have been widely applied in scientific and engineering fields. Solving integral and differential equations using physics-informed neural networks (PINNs) has emerged as an active and important area [34–37], attracting significant attention from researchers. However, data-driven PINNs rely on large amounts of data samples and are subject to approximation errors. Recently, a novel method called the neural network-based analytical solver [38, 39] was proposed to find analytical solutions of partial differential equations. The method in [40] employed explicit models of neural networks (NNs) as trial functions of the Fokker-Planck equation. Inspired by NNs which solve integer order partial differential equations, the motivation of this present paper is to show how analytical solutions of nonlinear space-time fPDEs can be constructed by the NN method, which has been shown to have major advantages in both computational accuracy and computational efficiency in solving analytical solutions of integer order nonlinear partial differential equations. To achieve this goal, we apply a fractional variable transformation, which actually provides us with a natural and straightforward way to convert a fractional partial differential equation into an integer order partial differential equation. The proposed method can be considered as a generalization of NNs under fractional derivatives circumstances. As illustrative examples, analytical solutions of the fractional Burgers equation, the fractional Burgers-Huxley equation, and the fractional Kdv-Burgers equation are obtained. The results demonstrate that the proposed method could successfully obtain analytical solutions of the equation without data samples. The fractional derivatives discussed in the present paper are in a modified Riemann-Liouville derivative sense.

The remainder of this present paper is organized as follows: in Section 2, we give the definition and properties of the conformable fractional derivative and describe essential steps of the fVTNNs; in Section 3, three applications of the method are provided; in Section 4, the conclusions of this paper are given.

2. Fractional variable transformation neural networks

We propose a fVTNN based on the NN method, and the main procedure of the method is described as follows.

Suppose that a space-time nonlinear fractional differential equation with independent variables (x, t) and the dependent variable u is formulated as follows:

$$P(u, D_t^\alpha u, D_x^\beta u, D_t^{2\alpha} u, D_x^{2\beta} u, \cdots) = 0, \quad 0 < \alpha, \beta \leq 1, \tag{2.1}$$

where $u(x, t)$ is the unknown function, P is a polynomial in u and its various partial derivatives, and $D_t^\alpha u, D_x^\beta u, D_t^{2\alpha} u, D_x^{2\beta} u$ are conformable fractional derivatives with respect to t and x, as defined below [41, 42].

Definition 2.1. Suppose $f : \mathbb{R} \times [0, +\infty) \to \mathbb{R}$ is a function. Then, the fractional conformable partial derivative of u of order α is defined as

$$D_t^\alpha f(t, x) = \lim_{\varepsilon \to 0} \frac{f(t + \varepsilon t^{1-\alpha}, x) - f(t, x)}{\varepsilon} \tag{2.2}$$

for all $t > 0$, $\alpha \in (0, 1)$, and D_t^α denotes the α order conformable fractional derivative operator with respect to t. The fractional derivative satisfies the properties presented in the following theorem [41,42].

Theorem 2.1. Consider $\alpha \in (0, 1]$, and suppose f and g are both α-differentiable at a point $t > 0$. Then,

1) $D_t^\alpha(af + bg) = aD_t^\alpha(f) + bD_t^\alpha(g)$, for all $a, b \in \mathbb{R}$;
2) $D_t^\alpha(t^p) = pt^{p-\alpha}$, for all $p \in \mathbb{R}$;
3) $D_t^\alpha(\lambda) = 0$, for all constant functions $f(t) = \lambda$;
4) $D_t^\alpha(fg) = fD_t^\alpha(g) + gD_t^\alpha(f)$;
5) $D_t^\alpha\left(\frac{f}{g}\right) = \frac{gD_t^\alpha(f) - fD_t^\alpha(g)}{g^2}$;
6) Moreover, if f is differentiable, then $D_t^\alpha(f)(t) = t^{1-\alpha}\frac{df}{dt}(t)$.

By fractional variable transformation,

$$T = \frac{t^\alpha}{\alpha}, \ X = \frac{x^\beta}{\beta}, \tag{2.3}$$

and we easily have

$$D_t^\alpha u = t^{1-\alpha} u_t = t^{1-\alpha} u_T T_t = t^{1-\alpha} u_T \cdot t^{\alpha-1} = u_T, \quad D_x^\alpha u = u_X \tag{2.4}$$

according to the properties of a conformable derivative.

Under Eq (2.4), Eq (2.1) can be rewritten as an integer order partial differential equation as follows:

$$P(u, u_T, u_X, u_{TT}, u_{XX}, \cdots) = 0. \tag{2.5}$$

Considering the powerful fitting ability of NNs, the explicit model of NNs is used as the trial function of Eq (2.5) in this paper. The NNs consist of one input layer, several hidden layers, and one output layer. The input layer is composed of independent variables of the considered problem. Every hidden layer consists of some neurons, two neurons in adjoining hidden layers are assigned to

a weight which is a real number not necessarily between zero and one, and every neuron in hidden layer is assigned to an activation function. The output of the NNs is composed of activation functions, weights, and biases. Suppose that solutions of Eq (2.5) could be expressed as explicit formulation of some functions provided by a NNs. To explain how a NN works, we take a relatively simple NNs, which has two hidden layers, as an example. The architecture of the NNs is denoted by Figure 1.

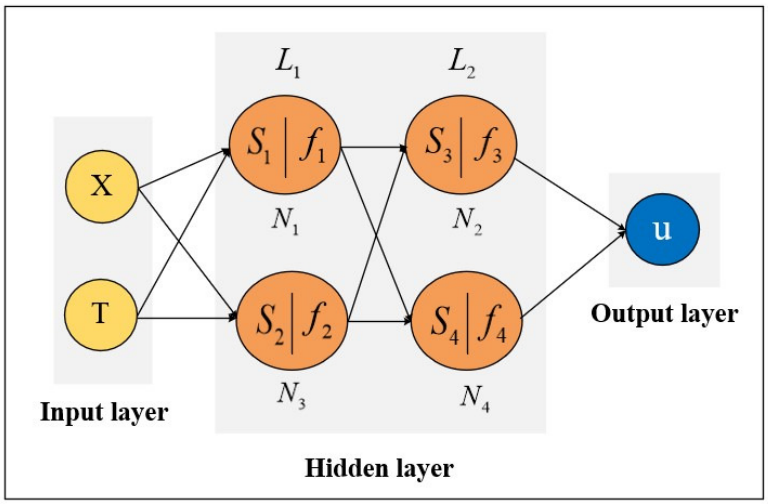

Figure 1. Architecture of a NNs.

In Figure 1, $T = t^{\alpha}/\alpha$ and $X = x^{\beta}/\beta$ in the input layer are independent variables of Eq (2.5). The first hidden layer L_1 and the second hidden layer L_2 both contain two neurons; these four neurons are denoted by N_1, N_2 and N_3, N_4. The ith neuron is assigned to an activation function $f_i, i = 1, 2, 3, 4$. Elementary functions such as fractions, trigonometric functions, exponential function, logarithmic function, hyperbolic functions, and even infinite series may be chosen as activation functions. These activation functions are generally obtained by analyzing the physical and mathematical properties of Eq (2.5). The inputs of the ith neuron are weighted and summed to generate sum S_i, i=1, 2, 3, 4. These sums has the following formulations:

$$\begin{aligned} S_1 &= w_{T1} \cdot T + w_{X1} \cdot X + b_1, \\ S_2 &= w_{T2} \cdot T + w_{X2} \cdot X + b_2, \\ S_3 &= w_{13} \cdot f_1(S_1) + w_{23} \cdot f_2(S_2) + b_3, \\ S_4 &= w_{14} \cdot f_1(S_1) + w_{24} \cdot f_2(S_2) + b_4, \end{aligned} \tag{2.6}$$

where w_{T1} denotes the weight between the input T and the first neuron L_1, w_{T2} denotes the weight between the input T and the second neuron L_2, w_{X1} denotes the weight between the input X and the first neuron L_1, w_{X2} denotes the weight between the input X and the second neuron L_2, w_{13} denotes the weight between the first neuron L_1 and the third neuron L_3, w_{23} denotes the weight between the second neuron L_2 and the third neuron L_3, w_{14} denotes the weight between the first neuron L_1 and the fourth neuron L_4, w_{24} denotes the weight between the second neuron and the fourth neuron L_4, and the symbols b_1, b_2, b_3, b_4 denote biases. In Eq (2.6), all the weights and biases are unknown and will be later determined by the NNs.

The output function $u = u(x,t)$ collects all the information of the NNs and acts as the potential analytical solution of Eq (2.5). Generally, the output function $u = u(x,t)$ has the following formulation:

$$u(x,t) = \begin{cases} w_{3u} \cdot f_3(S_3) + w_{4u} \cdot f_4(S_4) + b_5, \\ \quad \text{or} \\ w_{3u} \cdot f_3(S_3) \cdot w_{4u} \cdot f_4(S_4) + b_5, \end{cases} \tag{2.7}$$

where w_{3u} is the weight between the third neuron and the output function u, w_{4u} is the weight between the fourth neuron and the output function u, and b_5 is the bias. Parameters w_{3u}, w_{4u}, and b_5 are unknown and will be later determined by the NNs. Generally, the output function u is formulated as the weighed summation or weighed product of the output of the latest hidden layer.

For simplicity, we use the abbreviated notation *m-n-s-t* model to denote the NNs architecture, where m is the number of variables in the input layer, n and s are the numbers of neurons in the first and second hidden layers, respectively, and t is the number of output functions.

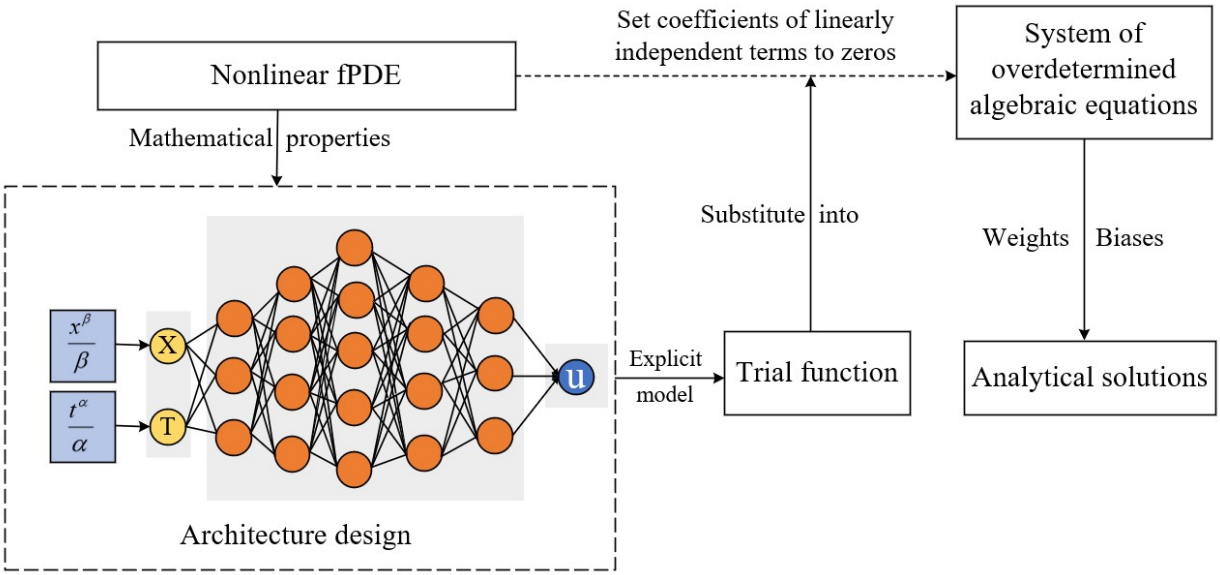

Figure 2. Flowchart of fVTNNs.

The flowchart of the proposed method is denoted by Figure 2. The main steps to solve the exact solutions of space-time fPDEs using fVTNNs are as follows:

Step 1: As illustrated in Figure 1, an appropriate NNs architecture is constructed for the target equation by determining the number of hidden layers, the number of neurons in each layer, and the activation function.

Step 2: Substituting the constructed trial function Eq (2.7) into the original equation Eq (2.5) yields a nonlinear algebraic equation.

Step 3: By combining like terms and equating the coefficients of linear independent functions about $f_i, i = 1, 2, 3, 4$ to zeros, a system of identities with respect to weights and biases are obtained.

Step 4: The relevant weights and biases are obtained by solving these equations by the symbol computational system Maple.

Step 5: Analytical solutions of Eq (2.5) are eventually founded by substituting these parameters back into Eq (2.7).

3. Applications

Fractional Burgers-type equations have extensive applications in fluid dynamics, heat conduction, diffusion, traffic flows, and other fields. The fVTNNs, described in Section 2, will be used to explore analytical solutions of nonlinear space-time fractional Burgers-type differential equations in the sequel.

3.1. Fractional Burgers equation

First, let us consider the nonlinear space-time fractional Burgers equation, which has the following form [43]:

$$D_t^{\alpha}u + au \cdot D_x^{\beta}u - bD_x^{2\beta}u = 0, \tag{3.1}$$

where $0 < \alpha, \beta \leq 1$, a and b are arbitrary constants, and u is the function of (x, t).

By the fractional variable transformation Eq (2.3), Eq (3.1) is rewritten as its integer order counterpart as follows:

$$u_T + au \cdot u_X - bu_{XX} = 0, \tag{3.2}$$

which is the classic Burgers equation.

Hyperbolic function solutions and exponential function interactive solutions of Eq (3.2) are discussed by the NN method, which is described as follows.

3.1.1. Hyperbolic function solutions

To obtain the potential hyperbolic function solutions of Eq (3.2), a NN that contains one hidden layer with two neurons is employed. The activation functions are taken as hyperbolic functions $\tanh(\cdot)$ and $\coth(\cdot)$. The NN architecture is shown in Table 1.

The mathematical formulation that corresponds to this model is as follows:

$$\begin{cases} S_1 = w_{t1} \cdot T + w_{x1} \cdot X + b_1, \\ S_2 = w_{t2} \cdot T + w_{x2} \cdot X + b_2, \\ u(x,t) = w_{1u} \cdot \tanh(S_1) + w_{2u} \cdot \coth(S_2) + b_3, \end{cases} \tag{3.3}$$

where the weights $w_{t1}, w_{x1}, w_{t2}, w_{x2}, w_{1u}, w_{2u}$ and biases b_1, b_2, b_3 are all unknown parameters to be determined later. The output function u is used as the weighed summation in the present.

Table 1. NNs architecture 1.

Layer	Neuron	Activation function
Input layer	T	-
	X	-
Hidden layer	1#	$\tanh(\cdot)$
	2#	$\coth(\cdot)$
Output layer	u	-

Based on the NN, the potential analytical solution $u(x,t)$ is formulated as follows:

$$u(x,t) = w_{1u}\tanh(w_{t1}T + w_{x1}X + b_1) + w_{2u}\coth(w_{t2}T + w_{x2}X + b_2) + b_3. \tag{3.4}$$

The potential analytical solution is viewed as a trial function to solve the fractional Burger equation. Substitute Eq (3.4) into Eq (3.2), and collect the left terms of the Eq (3.2) as polynomials of $\tanh(w_{t1}T + w_{x1}X + b_1)$ and $\coth(w_{t2}T + w_{x2}X + b_2)$. By letting the coefficients of $\tanh(w_{t1}T + w_{x1}X + b_1)$ and $\coth(w_{t2}T + w_{x2}X + b_2)$ be zeros, a system of algebraic equations that involve unknown weights and biases are obtained as follows:

$$\begin{cases} ab_3w_{1u}w_{x1} + ab_3w_{2u}w_{x2} + w_{1u}w_{t1} + w_{2u}w_{t2} = 0, \\ aw_{1u}^2w_{x1} + aw_{1u}w_{2u}w_{x2} + 2bw_{1u}w_{x1}^2 = 0, \\ aw_{1u}w_{2u}w_{x1} + aw_{2u}^2w_{x2} + 2bw_{2u}w_{x2}^2 = 0, \\ -aw_{1u}^2w_{x1} - 2bw_{1u}w_{x1}^2 = 0, \\ -aw_{2u}^2w_{x2} - 2bw_{2u}w_{x2}^2 = 0, \\ -aw_{1u}w_{2u}w_{x1} = 0, \\ -aw_{1u}w_{2u}w_{x2} = 0, \\ -ab_3w_{1u}w_{x1} - w_{1u}w_{t1} = 0, \\ -ab_3w_{2u}w_{x2} - w_{2u}w_{t2} = 0. \end{cases} \tag{3.5}$$

Solving Eq (3.5), two sets of effective solutions with respect to weights and biases are obtained, which corresponds to two analytical solutions of the fractional Burgers equation.

Case 1. Hyperbolic tangent solutions

$$\{a = a, b = b, b_3 = b_3, w_{1u} = -2bw_{x1}/a, w_{2u} = 0, w_{t1} = -ab_3w_{x1}, w_{t2} = w_{t2}, w_{x1} = w_{x1}, w_{x2} = w_{x2}\}. \tag{3.6}$$

The hyperbolic tangent solution to fractional Burgers equation that corresponds to this set of parameters is as follows:

$$u(x,t) = -\frac{2bw_{x1}}{a}\tanh\Big(-ab_3w_{x1}\cdot\frac{t^\alpha}{\alpha} + w_{x1}\cdot\frac{x^\beta}{\beta} + b_1\Big) + b_3. \tag{3.7}$$

Case 2. Hyperbolic cotangent solutions

$$\{a = a, b = b, b_3 = b_3, w_{1u} = 0, w_{2u} = -2bw_{x2}/a, w_{t1} = w_{t1}, w_{t2} = -ab_3w_{x2}, w_{x1} = w_{x1}, w_{x2} = w_{x2}\}. \tag{3.8}$$

The hyperbolic cotangent solution to the Eq (3.1) that corresponds to this set of parameters is as follows:

$$u(x,t) = -\frac{2bw_{x2}}{a}\coth\Big(-ab_3w_{x2}\cdot\frac{t^\alpha}{\alpha} + w_{x2}\cdot\frac{x^\beta}{\beta} + b_2\Big) + b_3. \tag{3.9}$$

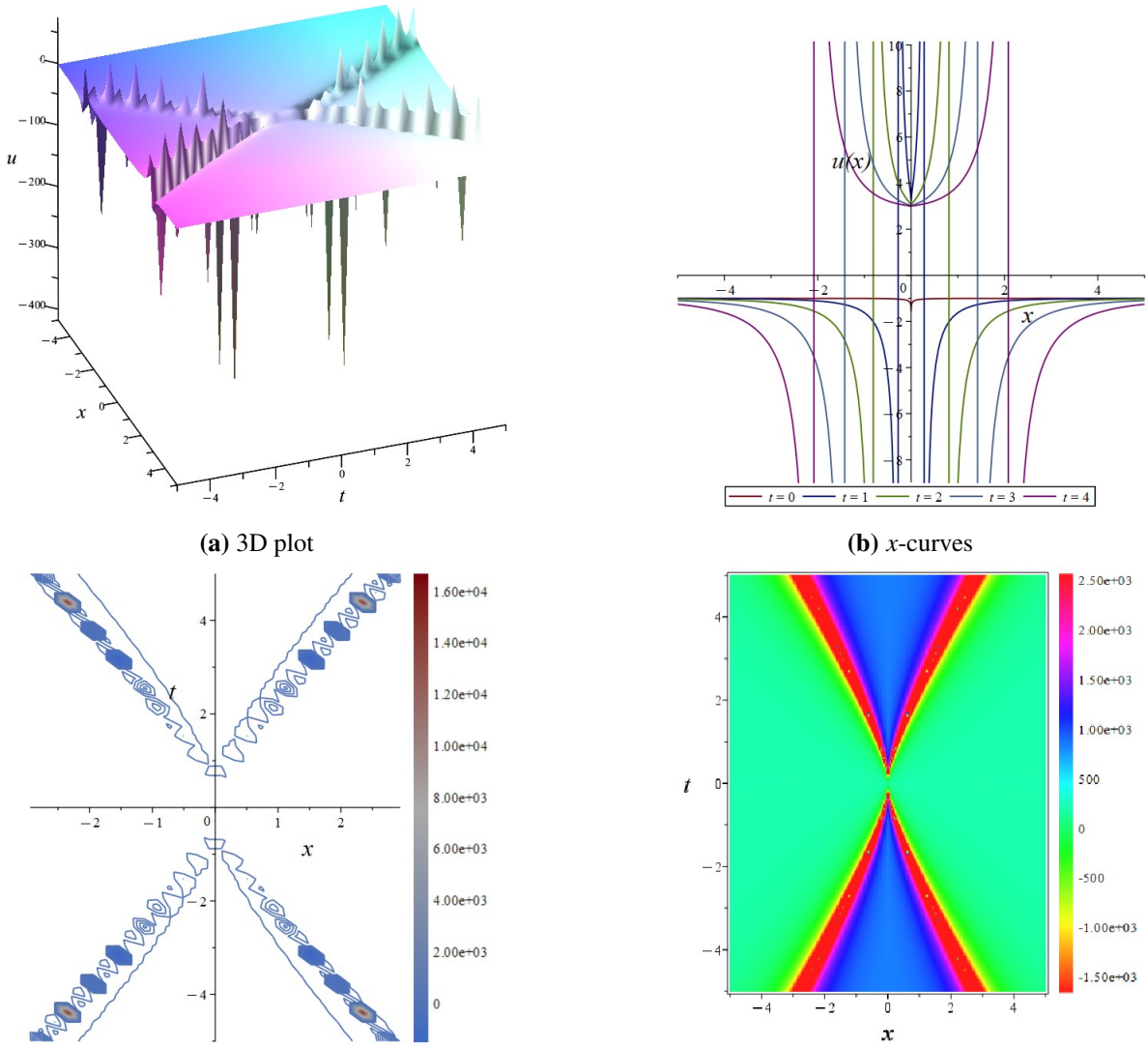

(a) 3D plot

(b) x-curves

(c) Contour plot

(d) Density plot

Figure 3. The 3D plot, curves plot, contour plot, and density plot of the solution Eq (3.9).

Under the parameter set $a = 1, b = 1, b_2 = 1, b_3 = 1, w_{x2} = 1$ and with fractional orders $\alpha = 0.4, \beta = 0.4$, the fractional Burgers equation exhibits characteristic dynamical features. A three-dimensional representation of the solution over the space-time domain $[-5, 5] \times [-5, 5]$ is provided in Figure 3(a). To further examine the local solution behavior, the spatial profile of $u(x, t)$ is displayed in Figure 3(b) for a fixed time interval $t \in [-5, 5]$. Additionally, Figure 3(c),(d) present the corresponding contour map and density distribution of the solution, respectively. Figure 3 systematically illustrates the form and evolutionary characteristics of an analytical solution to the fractional Burgers equation through four subfigures. The 3D surface plot clearly presents a typical nonlinear solitary wave structure with a sharp peak, which exhibits an evident dissipative decay and broadening over time. The 2D curve plot further reveals the spatial distribution of the waveform at specific moments, which is characterized by a steep front and a gradually decaying tail. On the other hand, contour and density plots, depict the propagation

path of the wave peak and the energy diffusion process on the x-t plane: contour lines are densely packed around the wave peak and gradually become sparser over time; and in the density plot, the bright peak region weakens and spreads as it evolves, shifting from bright to dark colors. Collectively, these visualizations intuitively verify the waveform evolution laws that result from the interaction between the nonlinear term and the fractional dissipative term in the fractional Burgers equation, namely, the nonlinear effect tends to maintain the waveform, while the fractional dissipation leads to its attenuation and dispersion. This waveform evolution characteristic holds significant application value in describing physical systems with complex microstructures (such as porous media and fractal materials) or memory properties (such as viscoelastic fluids). Its slow decay and unique diffusion patterns provide an intuitive mathematical model to explain anomalous transport phenomena in such systems.

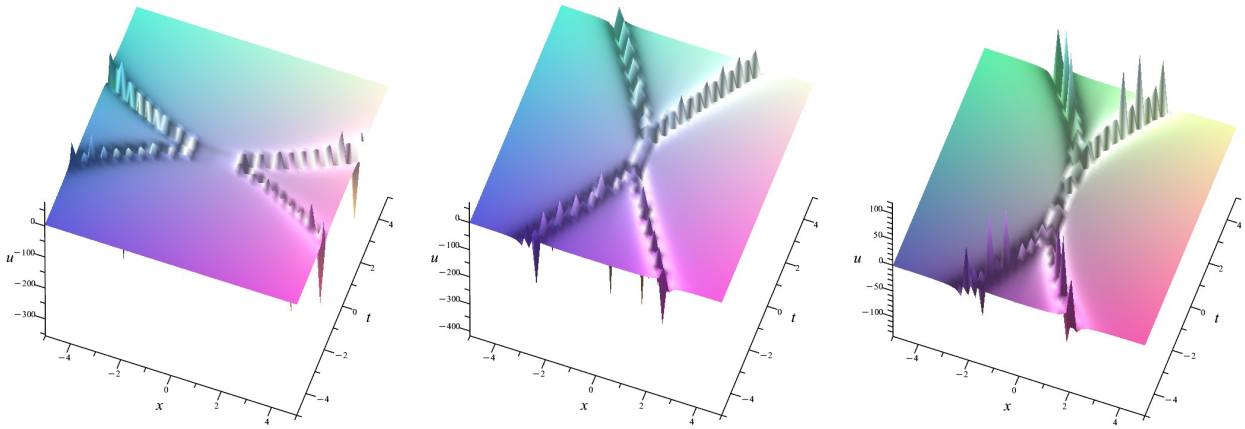

(a) $\alpha = 0.2, \beta = 0.4$ **(b)** $\alpha = 0.4, \beta = 0.4$ **(c)** $\alpha = 0.6, \beta = 0.4$

Figure 4. The 3D plots of the solution Eq (3.9) at different fractional derivative values.

Figure 4 visually illustrates the three-dimensional waveform evolution of the analytical solution Eq (3.9) to the Eq (3.1) under different fractional derivative values. A comparison among the three parameter sets reveals that when β is fixed at 0.4, the temporal evolution rate of the waveform significantly accelerates as the time fractional order α increases from 0.2 to 0.6. The diffusion behavior of the wave peak along the time axis becomes more pronounced, which indicates that α primarily regulates the temporal dynamics and memory effects of the solution. The spatial fractional order β mainly influences the smoothness and decay characteristics of the waveform in the spatial dimension. This demonstrates that α and β jointly determine the dissipation, dispersion, and nonlinear balance in the fractional system, thereby governing the spatiotemporal propagation patterns and structural stability of the solution.

3.1.2. Exponential function interactive solutions

To obtain the potential exponential function interactive solutions of Eq (3.2), a NN that contains containing two hidden layers, where each layer has two neurons, is designed. The activation functions of two neurons of the first hidden layer are chosen as the exponential function $\exp(\cdot)$. The activation functions of the second hidden layer are chosen as $(\cdot)$ and $1/(\cdot)$. The architecture of the NN is shown in Table 2.

Table 2. NNs architecture 2.

Layer	Neuron	Activation function
Input layer	X	-
	T	-
The first hidden layer	1#	$\exp(\cdot)$
	2#	$\exp(\cdot)$
The second hidden layer	3#	$(\cdot)$
	4#	$1/(\cdot)$
Output layer	u	-

The mathematical formulation that corresponds to this model is as follows:

$$\begin{cases} S_1 = w_{t1}T + w_{x1}X + b_1, \\ S_2 = w_{t2}T + w_{x2}X + b_2, \\ S_3 = w_{13} \cdot \mathrm{e}^{S_1} + w_{23} \cdot \mathrm{e}^{S_2} + b_3, \\ S_4 = w_{14} \cdot \mathrm{e}^{S_1} + w_{24} \cdot \mathrm{e}^{S_2} + b_4, \\ u(x,t) = w_{3u} \cdot S_3 \cdot w_{4u} \cdot \frac{1}{S_4} + b_5, \end{cases} \tag{3.10}$$

where the weights $w_{t1}, w_{x1}, w_{t2}, w_{x2}, w_{13}, w_{23}, w_{14}, w_{24}, w_{3u}, w_{4u}$ and biases b_1, b_2, b_3, b_4, b_5 are all unknown parameters to be later determined.

Based on the NNs, the potential analytical solution $u(x,t)$ is formulated as follows:

$$u(x,t) = \frac{w_{3u}w_{4u}\left(w_{13} \cdot \mathrm{e}^{w_{t1}T+w_{x1}X+b_1} + w_{23} \cdot \mathrm{e}^{w_{t2}T+w_{x2}X+b_2} + b_3\right)}{w_{14} \cdot \mathrm{e}^{w_{t1}T+w_{x1}X+b_1} + w_{24} \cdot \mathrm{e}^{w_{t2}T+w_{x2}X+b_2} + b_4} + b_5. \tag{3.11}$$

The potential analytical solution Eq (3.11) is thought as a trial function to solve the fractional Burger equation. We substitute Eq (3.11) into Eq (3.2), and organize the left terms of Eq (3.2) as polynomials of $\mathrm{e}^{w_{t1}T+w_{x1}X+b_1}$ and $\mathrm{e}^{w_{t2}T+w_{x2}X+b_2}$. By letting coefficients of linear independent terms about $\mathrm{e}^{w_{t1}T+w_{x1}X+b_1}$ and $\mathrm{e}^{w_{t2}T+w_{x2}X+b_2}$ be zeros, a system of algebraic equations that involve unknown weights and biases are obtained. Solving these equations, we can obtain many sets of effective solutions of weights and biases, which correspond to analytical solutions of the fractional Burgers equation. According to the way in which the NN connects, all effective solutions of Eq (3.1) are classified into two cases as follows.

Case 1. 2-2-2-1 model

Case 1.1

$$\begin{aligned} &\{a = a, b = b, b_3 = b_4 = 0, w_{13} = w_{14}(aw_{23}w_{3u}w_{4u} - 2bw_{24}w_{x1} + 2bw_{24}w_{x2})/(aw_{24}w_{3u}w_{4u}), \\ &b_5 = b_5, w_{14} = w_{14}, w_{23} = w_{23}, w_{24} = w_{24}, w_{3u} = w_{3u}, w_{4u} = w_{4u}, w_{t2} = w_{t2}, w_{x1} = w_{x1}, \\ &w_{x2} = w_{x2}, w_{t1} = -(aw_{23}w_{3u}w_{4u}w_{x1} - aw_{23}w_{3u}w_{4u}w_{x2} + ab_5w_{24}w_{x1} - ab_5w_{24}w_{x2} \\ &-bw_{24}w_{x1}^2 + 2bw_{24}w_{x1}w_{x2} - bw_{24}w_{x2}^2 - w_{24}w_{t2})/w_{24}\Big\}. \end{aligned} \tag{3.12}$$

The exponential function interactive solutions to Eq (3.1) which correspond to the above set of parameters is as as follows:

$$u(x,t)=\frac{w_{3u}w_{4u}\left(w_{13}\cdot \mathrm{e}^{w_{t1}T+w_{x1}X+b_1}+w_{23}\cdot \mathrm{e}^{w_{t2}T+w_{x2}X+b_2}\right)}{w_{14}\cdot \mathrm{e}^{w_{t1}T+w_{x1}X+b_1}+w_{24}\cdot \mathrm{e}^{w_{t2}T+w_{x2}X+b_2}}+b_5, \tag{3.13}$$

where $T=t^{\alpha}/\alpha$, $X=x^{\beta}/\beta$, and w_{13}, w_{t1} are indicated in Eq (3.12).

Case 1.2

$$\begin{aligned}&\{a=a,b=b,b_3=b_4=0,b_5=b_5,w_{13}=w_{13},w_{14}=w_{14},w_{23}=w_{23},w_{24}=w_{24},w_{3u}=w_{3u},\\&w_{4u}=w_{4u},w_{t1}=w_{t2},w_{t2}=w_{t2},w_{x1}=w_{x2},w_{x2}=w_{x2}\}.\end{aligned} \tag{3.14}$$

The exponential function interactive solutions to Eq (3.1) which correspond to the above set of parameters is as as follows:

$$u(x,t)=\frac{w_{3u}w_{4u}\left(w_{13}\mathrm{e}^{Tw_{t2}+Xw_{x2}+b_1}+w_{23}\mathrm{e}^{Tw_{t2}+Xw_{x2}+b_2}\right)}{w_{14}\mathrm{e}^{Tw_{t2}+Xw_{x2}+b_1}+w_{24}\mathrm{e}^{Tw_{t2}+Xw_{x2}+b_2}}+b_5, \tag{3.15}$$

where $T=t^{\alpha}/\alpha$, and $X=x^{\beta}/\beta$.

Case 1.3

$$\begin{aligned}&\{a=a,b=b,b_3=b_3,b_4=b_4,w_{14}=w_{14},w_{24}=w_{24},w_{3u}=w_{3u},w_{4u}=w_{4u},w_{t2}=w_{t2},\\&b_5=-(ab_3w_{3u}w_{4u}w_{x2}-bb_4w_{x2}^2+b_4w_{t2})/(ab_4w_{x2}),w_{t1}=(bw_{x1}w_{x2}-bw_{x2}^2+w_{t2})w_{x1}/w_{x2},\\&w_{x1}=w_{x1},w_{x2}=w_{x2},w_{13}=w_{14}(ab_3w_{3u}w_{4u}-2bb_4w_{x1})/(ab_4w_{3u}w_{4u}),\\&w_{23}=w_{24}(ab_3w_{3u}w_{4u}-2bb_4w_{x2})/(ab_4w_{3u}w_{4u})\}.\end{aligned} \tag{3.16}$$

Therefore, the exponential function interactive solutions to Eq (3.1) which correspond to the above set of parameters is as follows:

$$u(x,t)=\frac{w_{3u}w_{4u}\left(w_{13}\cdot \mathrm{e}^{w_{t1}T+w_{x1}X+b_1}+w_{23}\cdot \mathrm{e}^{w_{t2}T+w_{x2}X+b_2}+b_3\right)}{w_{14}\cdot \mathrm{e}^{w_{t1}T+w_{x1}X+b_1}+w_{24}\cdot \mathrm{e}^{w_{t2}T+w_{x2}X+b_2}+b_4}+b_5, \tag{3.17}$$

where $T=t^{\alpha}/\alpha$, $X=x^{\beta}/\beta$, and $b_5, w_{13}, w_{23}, w_{t1}$ are indicated in Eq (3.16).

Case 1.4

$$\begin{aligned}&\{a=a,b=b,b_4=b_4,w_{23}=w_{23},w_{24}=w_{24},w_{3u}=w_{3u},w_{4u}=w_{4u},w_{t2}=w_{t2},w_{x2}=w_{x2},\\&b_3=b_4(aw_{23}w_{3u}w_{4u}+2bw_{24}w_{x2})/(aw_{24}w_{3u}w_{4u}),w_{t1}=2bw_{x2}^2+2w_{t2},w_{x1}=2w_{x2},\\&b5=-(aw_{23}w_{3u}w_{4u}w_{x2}+bw_{24}w_{x2}^2+w_{24}w_{t2})/(w_{24}w_{x2}a),w_{14}=w_{14},\\&w_{13}=w_{14}(aw_{23}w_{3u}w_{4u}-2bw_{24}w_{x2})/(aw_{24}w_{3u}w_{4u})\}.\end{aligned} \tag{3.18}$$

Therefore, the exponential function interactive solution to Eq (3.1) which correspond to the above set of parameters is as follows:

$$u(x,t)=\frac{w_{3u}w_{4u}\left(w_{13}\cdot \mathrm{e}^{w_{t1}T+2w_{x2}X+b_1}+w_{23}\cdot \mathrm{e}^{w_{t2}T+w_{x2}X+b_2}+b_3\right)}{w_{14}\cdot \mathrm{e}^{w_{t1}T+2w_{x2}X+b_1}+w_{24}\cdot \mathrm{e}^{w_{t2}T+w_{x2}X+b_2}+b_4}+b_5, \tag{3.19}$$

where $T = t^\alpha/\alpha$, $X = x^\beta/\beta$, and b_3, b_5, w_{13}, w_{t1} are indicated in Eq (3.18).

Case 1.5

$$\begin{aligned}&\{a = a, b = b, b_3 = b_4 w_{13}/w_{14}, b_4 = b_4, w_{13} = w_{13}, w_{14} = w_{14}, w_{3u} = w_{3u}, w_{4u} = w_{4u},\\ &b_5 = -(a w_{13} w_{3u} w_{4u} w_{x2} - b w_{14} w_{x2}^2 + w_{14} w_{t2})/(w_{14} w_{x2} a), w_{t2} = w_{t2}, w_{x2} = w_{x2},\\ &w_{23} = w_{24}(a w_{13} w_{3u} w_{4u} - 2b w_{14} w_{x2})/(a w_{14} w_{3u} w_{4u}), w_{24} = w_{24}, w_{t1} = w_{x1} = 0\}.\end{aligned} \tag{3.20}$$

$$u(x,t) = \frac{-w_{24}\left(b w_{x2}^2 + w_{t2}\right)\mathrm{e}^{T w_{t2} + X w_{x2} + b_2} - \left(w_{14}\mathrm{e}^{b_1} + b_4\right)\left(-b w_{x2}^2 + w_{t2}\right)}{a\left(w_{14}\mathrm{e}^{b_1} + w_{24}\mathrm{e}^{T w_{t2} + X w_{x2} + b_2} + b_4\right) w_{x2}}, \tag{3.21}$$

where $T = t^\alpha/\alpha$, and $X = x^\beta/\beta$.

Case 1.6

$$\begin{aligned}&\{a = a, b = b, b_3 = b_4 w_{23}/w_{24}, b_4 = b_4, w_{t1} = w_{t1}, w_{t2} = w_{x2} = 0, w_{14} = w_{14}, w_{23} = w_{23},\\ &b_5 = -(a w_{23} w_{3u} w_{4u} w_{x1} - b w_{24} w_{x1}^2 + w_{24} w_{t1})/(w_{24} w_{x1} a), w_{24} = w_{24}, w_{3u} = w_{3u},\\ &w_{13} = w_{14}(a w_{23} w_{3u} w_{4u} - 2b w_{24} w_{x1})/(a w_{24} w_{3u} w_{4u}), w_{x1} = w_{x1}, w_{4u} = w_{4u}\}\end{aligned} \tag{3.22}$$

$$u(x,t) = \frac{-w_{14}\left(b w_{x1}^2 + w_{t1}\right)\mathrm{e}^{T w_{t1} + X w_{x1} + b_1} - \left(w_{24}\mathrm{e}^{b_2} + b_4\right)\left(-b w_{x1}^2 + w_{t1}\right)}{a\left(w_{14}\mathrm{e}^{T w_{t1} + X w_{x1} + b_1} + w_{24}\mathrm{e}^{b_2} + b_4\right) w_{x1}}, \tag{3.23}$$

where $T = t^\alpha/\alpha$, and $X = x^\beta/\beta$.

Case 2. 2-1-2-1 model

Case 2.1

$$\begin{aligned}&\{a = a, b = b, b_3 = b_3, b_4 = b_4, b_5 = b_5, w_{24} = w_{24}, w_{3u} = w_{3u}, w_{x1} = w_{x1},\\ &w_{23} = w_{24}(a b_3 w_{3u} w_{4u} - 2b b_4 w_{x2})/(a b_4 w_{3u} w_{4u}), w_{4u} = w_{4u}, w_{x2} = w_{x2},\\ &w_{t2} = -w_{x2}(a b_3 w_{3u} w_{4u} + a b_4 b_5 - b b_4 w_{x2})/b_4, w_{t1} = w_{t1}, w_{13} = w_{14} = 0\}.\end{aligned} \tag{3.24}$$

$$u(x,t) = \frac{w_{3u} w_{4u}\left(w_{23} \cdot \mathrm{e}^{w_{t2} T + w_{x2} X + b_2} + b_3\right)}{w_{24} \cdot \mathrm{e}^{w_{t2} T + w_{x2} X + b_2} + b_4} + b_5, \tag{3.25}$$

where $T = t^\alpha/\alpha$, $X = x^\beta/\beta$, and w_{23}, w_{t2} are indicated in Eq (3.24).

Case 2.2

$$\begin{aligned}&\{a = a, b = b, b_3 = b_4(a w13 w_{3u} w_{4u} + 2b w_{14} w_{x1})/(a w_{14} w_{3u} w_{4u}), w_{t2} = w_{t2}, w_{x2} = w_{x2},\\ &b_4 = b_4, b_5 = b_5, w_{13} = w_{13}, w_{14} = w_{14}, w_{23} = 0, w_{24} = 0, w_{x1} = w_{x1}, w_{3u} = w_{3u},\\ &w_{4u} = w_{4u}, w_{t1} = -w_{x1}(a w_{13} w_{3u} w_{4u} + a b_5 w_{14} + b w_{14} w_{x1})/w_{14}\}.\end{aligned} \tag{3.26}$$

$$u(x,t) = \frac{w_{3u} w_{4u}\left(w_{13}\mathrm{e}^{-\frac{T w_{x1}(a w_{13} w_{3u} w_{4u} + a b_5 w_{14} + b w_{14} w_{x1})}{w_{14}} + X w_{x1} + b_1} + \frac{b_4(a w_{13} w_{3u} w_{4u} + 2b w_{14} w_{x1})}{a w_{14} w_{3u} w_{4u}}\right)}{w_{14}\mathrm{e}^{-\frac{T w_{x1}(a w_{13} w_{3u} w_{4u} + a b_5 w_{14} + b w_{14} w_{x1})}{w_{14}} + X w_{x1} + b_1} + b_4} + b_5, \tag{3.27}$$

where $T = t^\alpha/\alpha$, and $X = x^\beta/\beta$.

3.1.3. Triangular periodic solutions

To obtain the potential triangular periodic solutions of Eq (3.2), a NN that contains two hidden layers, where each layer has two neurons, is designed. The activation functions of two neurons of the first hidden layer are chosen as the trigonometric function tan(·). The activation functions of the second hidden layer are chosen as (·). The architecture of the NN is shown in Table 3.

Table 3. NNs architecture 3.

Layer	Neuron	Activation function
Input layer	X	-
	T	-
The first hidden layer	1#	$\tan(\cdot)$
	2#	$\tan(\cdot)$
The second hidden layer	3#	$(\cdot)$
	4#	$(\cdot)$
Output layer	u	-

The mathematical formulation that corresponds to this model is as follows:

$$\begin{aligned} u(x,t) = &\left(w_{13}\tan(Tw_{t1} + Xw_{x1} + b_1) + w_{23}\tan(Tw_{t2} + Xw_{x2} + b_2) + b_3\right) w_{3u} \\ &+ \left(w_{14}\tan(Tw_{t1} + Xw_{x1} + b_1) + w_{24}\tan(Tw_{t2} + Xw_{x2} + b_2) + b_4\right) w_{4u} + b_5. \end{aligned} \tag{3.28}$$

The potential analytical solution Eq (3.28) is thought as a trial function to solve the fractional Burger equation. We substitute Eq (3.28) into Eq (3.2), and organize the left terms of Eq (3.2) as polynomials of $\tan(w_{t1}T + w_{x1}X + b_1)$ and $\tan(w_{t2}T + w_{x2}X + b_2)$. By letting the coefficients of linear independent terms be zeros, a system of algebraic equations that involve unknown weights and biases are obtained. Solving these equations, we can obtain many sets of effective solutions of weights and biases, which corresponds to analytical solutions of the fractional Burgers equation. According to the way in which the NN connects, all effective solutions of Eq (3.1) are classified into two cases as follows.

Case 1. 2-1-2-1 model

Case 1.1

$$\begin{aligned} &\{a = a, b = a\left(w_{23}w_{3u} + w_{24}w_{4u}\right)/2w_{x2}, b_3 = b_3, b_4 = b_4, w_{13} = -w_{14}w_{4u}/w_{3u}, w_{14} = w_{14}, \\ &b_5 = -a\left(b_3w_{3u} + b_4w_{4u}\right)w_{x2} - w_{t2}/aw_{x2}, w_{23} = w_{23}, w_{24} = w_{24}, w_{3u} = w_{3u}, w_{4u} = w_{4u}, \\ &w_{t1} = 0, w_{t2} = w_{t2}, w_{x1} = 0, w_{x2} = w_{x2}\}. \end{aligned} \tag{3.29}$$

$$u(x,t) = \frac{aw_{x2}\left(w_{23}w_{3u} + w_{24}w_{4u}\right)\tan(Tw_{t2} + Xw_{x2} + b_2) - w_{t2}}{aw_{x2}}, \tag{3.30}$$

where $T = t^{\alpha}/\alpha$, and $X = x^{\beta}/\beta$.

Case 1.2

$$\begin{aligned}&\{a = a, b = a\left(w_{13}w_{3u} + w_{14}w_{4u}\right)/2w_{x1}, b_3 = b_3, b_4 = b_4, w_{13} = w_{13}, w_{14} = w_{14},\\ &b_5 = -a\left(b_3w_{3u} + b_4w_{4u}\right)w_{x1} - w_{t1}/aw_{x1}, w_{23} = -w_{24}w_{4u}/w_{3u}, w_{24} = w_{24},\\ &w_{3u} = w_{3u}, w_{4u} = w_{4u}, w_{t1} = w_{t1}, w_{t2} = 0, w_{x1} = w_{x1}, w_{x2} = 0\}.\end{aligned} \tag{3.31}$$

$$u(x,t) = \frac{aw_{x1}\left(w_{13}w_{3u} + w_{14}w_{4u}\right)\tan(Tw_{t1} + Xw_{x1} + b_1) - w_{t1}}{aw_{x1}}, \tag{3.32}$$

where $T = t^{\alpha}/\alpha$, and $X = x^{\beta}/\beta$.

Case 2. 2-1-1-1 model

Case 2.1

$$\begin{aligned}&\{a = a, b = aw_{24}w_{4u}/2w_{x2}, b_3 = b_3, b_4 = b_4, w_{13} = w_{13}, b_5 = -ab_4w_{4u}w_{x2} - w_{t2}/aw_{x2},\\ &w_{14} = 0, w_{23} = w_{23}, w_{24} = w_{24}, w_{3u} = 0, w_{4u} = w_{4u}, w_{t1} = 0, w_{t2} = w_{t2}, w_{x1} = 0, w_{x2} = w_{x2}\}.\end{aligned} \tag{3.33}$$

$$u(x,t) = \frac{aw_{13}w_{x1}\left(w_{3u} + w_{4u}\right)\tan(Tw_{t1} + Xw_{x1} + b_1) - w_{t1}}{aw_{x1}}, \tag{3.34}$$

where $T = t^{\alpha}/\alpha$, and $X = x^{\beta}/\beta$.

Case 2.2

$$\begin{aligned}&\{a = a, b = aw_{24}w_{4u}/2w_{x2}, b_3 = b_3, b_4 = -ab_5w_{x2} - w_{t2}/aw_{4u}w_{x2}, w_{13} = w_{13}, b_5 = b_5,\\ &w_{14} = 0, w_{23} = w_{23}, w_{24} = w_{24}, w_{3u} = 0, w_{4u} = w_{4u}, w_{t1} = w_{t1}, w_{t2} = w_{t2}, w_{x1} = 0, w_{x2} = w_{x2}\}.\end{aligned} \tag{3.35}$$

$$u(x,t) = \frac{\tan(Tw_{t2} + Xw_{x2} + b_2)\,aw_{24}w_{4u}w_{x2} - w_{t2}}{aw_{x2}}, \tag{3.36}$$

where $T = t^{\alpha}/\alpha$, and $X = x^{\beta}/\beta$.

3.1.4. Rational function solutions

To obtain the potential rational function of Eq (3.2), a NN that contains two hidden layers, where each layer has two neurons, is designed. The activation functions of two neurons of the first hidden layer are chosen as $(\cdot)$. The activation functions of the second hidden layer are chosen as $(\cdot)$ and $1/(\cdot)$. The architecture of the NN is shown in Table 4.

Table 4. NNs architecture 4.

Layer	Neuron	Activation function
Input layer	X	-
	T	-
The first hidden layer	1#	$(\cdot)$
	2#	$(\cdot)$
The second hidden layer	3#	$(\cdot)$
	4#	$1/(\cdot)$
Output layer	u	-

The mathematical formulation that corresponds to this model is as follows:

$$\begin{aligned} u(x,t) = \; & w_{3u}\left(\left(Tw_{t1}+Xw_{x1}+b_1\right)w_{13}+\left(Tw_{t2}+Xw_{x2}+b_2\right)w_{23}+b_3\right) \\ & + \frac{w_{4u}}{\left(Tw_{t1}+Xw_{x1}+b_1\right)w_{14}+\left(Tw_{t2}+Xw_{x2}+b_2\right)w_{24}+b_4}+b_5. \end{aligned} \tag{3.37}$$

By substituting Eq (3.37) into Eq (3.2), combining like terms, and extracting the coefficients, a system of nonlinear algebraic equations is obtained. Solving this system of nonlinear algebraic equations using the Maple symbolic computation software yields the corresponding coefficient solutions.

Case 1. 2-2-2-1 model

Case 1.1

$$\begin{aligned} &\{a=a, b=b, b_1=b_1, b_2=b_2, b_3=b_3, b_4=b_4, b_5=b_5, w_{13}=w_{13}, w_{14}=w_{14}, w_{23}=w_{23}, \\ &w_{24}=-b_1w_{14}-b_4/b_2, w_{3u}=w_{3u}, w_{4u}=w_{4u}, w_{t1}=w_{t1}, w_{t2}=b_2w_{14}w_{t1}/b_1w_{14}+b_4, \\ &w_{x1}=w_{x1}, w_{x2}=b_2w_{14}w_{x1}/b_1w_{14}+b_4\}. \end{aligned} \tag{3.38}$$

$$\begin{aligned} u(x,t) = \; & w_{3u}\left(\left(Tw_{t1}+Xw_{x1}+b_1\right)w_{13}+\left(\frac{Tb_2w_{14}w_{t1}}{b_1w_{14}+b_4}+\frac{Xb_2w_{14}w_{x1}}{b_1w_{14}+b_4}+b_2\right)w_{23}+b_3\right) \\ & + \frac{w_{4u}}{\left(Tw_{t1}+Xw_{x1}+b_1\right)w_{14}-\frac{\left(\frac{Tb_2w_{14}w_{t1}}{b_1w_{14}+b_4}+\frac{Xb_2w_{14}w_{x1}}{b_1w_{14}+b_4}+b_2\right)\left(b_1w_{14}+b_4\right)}{b_2}+b_4}+b_5, \end{aligned} \tag{3.39}$$

where $T=t^{\alpha}/\alpha$, and $X=x^{\beta}/\beta$.

Case 1.2

$$\begin{aligned} &\{a=a, b=b, b_1=b_1, b_2=b_2, b_3=b_3, b_4=b_4, b_5=b_5, w_{13}=w_{13}, w_{14}=w_{14}, w_{23}=w_{23}, \\ &w_{24}=w_{24}, w_{3u}=w_{3u}, w_{4u}=-2bw_{t1}\left(w_{13}w_{24}+w_{14}w_{23}\right)/\left(w_{3u}b_1w_{13}+w_{3u}b_2w_{23}+w_{3u}b_3+b_5\right) \\ &\cdot a^2w_{23}, w_{t1}=w_{t1}, w_{t2}=-w_{t1}w_{13}/w_{23}, w_{x1}=-w_{t1}/\left(w_{3u}b_1w_{13}+w_{3u}b_2w_{23}+w_{3u}b_3+b_5\right)a, \\ &w_{x2}=w_{13}w_{t1}/\left(w_{3u}b_1w_{13}+w_{3u}b_2w_{23}+w_{3u}b_3+b_5\right)aw_{23}\}. \end{aligned} \tag{3.40}$$

$$\begin{aligned} u(x,t) = & -\frac{2bw_{t1}\left(w_{13}w_{24}-w_{14}w_{23}\right)}{\left(w_{3u}b_1w_{13}+w_{3u}b_2w_{23}+w_{3u}b_3+b_5\right)a^2w_{23}\left(\xi_1w_{14}+\xi_2w_{24}+b_4\right)} \\ & + w_{3u}\left(\xi_1w_{13}+\xi_2w_{23}+b_3\right)+b_5, \end{aligned} \tag{3.41}$$

where $\xi_1=Tw_{t1}+Xw_{x1}+b_1, \xi_2=Tw_{t2}+Xw_{x2}+b_2$, $T=t^{\alpha}/\alpha$, and $X=x^{\beta}/\beta$.

Case 2. 2-2-1-1 model

Case 2.1

$$\begin{aligned} &\{a=a, b=b, b_1=b_1, b_2=b_2, b_3=b_3, b_4=b_4, b_5=b_5, w_{13}=w_{13}, w_{14}=w_{14}, w_{23}=w_{23}, \\ &w_{24}=w_{24}, w_{3u}=0, w_{4u}=2b\left(w_{14}w_{t1}+w_{24}w_{t2}\right)/a^2b_5, w_{t1}=w_{t1}, w_{t2}=w_{t2}, w_{x1}=w_{x1}, \\ &w_{x2}=-ab_5w_{14}w_{x1}-w_{14}w_{t1}-w_{24}w_{t2}/b_5aw_{24}\}. \end{aligned} \tag{3.42}$$

$$u(x,t) = \frac{2b\left(w_{14}w_{t1} + w_{24}w_{t2}\right)}{a\left(b_5\left(\left(Tw_{t2} + b_2\right)w_{24} + Tw_{14}w_{t1} + b_1w_{14} + b_4\right)a - X\left(w_{14}w_{t1} + w_{24}w_{t2}\right)\right)} + b_5, \tag{3.43}$$

where $T = t^\alpha/\alpha$, and $X = x^\beta/\beta$.

Case 2.2

$$\begin{aligned}&\{a = a, b = b, b_1 = b_1, b_2 = b_2, b_3 = b_3, b_4 = b_4, b_5 = b_5, w_{13} = 0, w_{14} = w_{14}, w_{24} = w_{24},\\ &w_{23} = 0, w_{3u} = w_{3u}, w_{4u} = 2b\left(w_{14}w_{t1} + w_{24}w_{t2}\right)/a^2\left(w_{3u}b_3 + b_5\right), w_{t1} = w_{t1}, w_{t2} = w_{t2},\\ &w_{x1} = w_{x1}, w_{x2} = -ab_3w_{14}w_{3u}w_{x1} - ab_5w_{14}w_{x1} - w_{14}w_{t1} - w_{24}w_{t2}/aw_{24}\left(w_{3u}b_3 + b_5\right)\}.\end{aligned} \tag{3.44}$$

$$\begin{aligned}u(x,t) = &\frac{2b\left(w_{14}w_{t1} + w_{24}w_{t2}\right)}{a\left(\left(w_{3u}b_3 + b_5\right)\left(Tw_{14}w_{t1} + w_{24}Tw_{t2} + b_1w_{14} + w_{24}b_2 + b_4\right)a - X\left(w_{14}w_{t1} + w_{24}w_{t2}\right)\right)}\\ &+ w_{3u}b_3 + b_5,\end{aligned} \tag{3.45}$$

where $T = t^\alpha/\alpha$, and $X = x^\beta/\beta$.

3.2. Fractional Burgers-Huxley equation

The second instructive example to illustrate the fractional variable transformation NN method is the fractional nonlinear Burgers-Huxley equation, which is written as follows:

$$D_t^\alpha u + \frac{3}{k}u \cdot D_x^\beta u + D_x^{2\beta}u + cu + u^2 + u^3 = 0, \tag{3.46}$$

where $0 < \alpha, \beta \leq 1$, and k, c are arbitrary constants, and u is the function of (x, t).

By the fractional variable transformation, Eq (3.46) is rewritten as follows:

$$u_T + \frac{3}{k}u \cdot u_X + u_{XX} + cu + u^2 + u^3 = 0. \tag{3.47}$$

Additionally, fractional hyperbolic function solutions and exponential function interactive solutions of Eq (3.47) will be explored by the NN method, and are described below.

3.2.1. Hyperbolic function solutions

By the same discussion as Subsection 3.1.1, two sets of effective solutions about weights and biases are obtained as follows.

Case 1.

$$\{c = 2/9, k = 1, b_3 = -1/3, w_{1u} = w_{t1} = w_{x1} = -1/6, w_{2u} = 1/6, w_{t2} = w_{x2} = 1/6\}. \tag{3.48}$$

In this case, Eq (3.46) can be written as a special form of fractional Burgers-Huxley equation as follows:

$$D_t^\alpha u + 3u \cdot D_x^\beta u + D_x^{2\beta}u + \frac{2}{9}u + u^2 + u^3 = 0. \tag{3.49}$$

The fractional hyperbolic function solutions to Eq (3.49) which correspond to this set of parameters is as follows:

$$u(x,t) = -\frac{1}{6}\tanh\Big(-\frac{t^\alpha}{6\alpha} - \frac{x^\beta}{6\beta} + b_1\Big) + \frac{1}{6}\coth\Big(\frac{t^\alpha}{6\alpha} + \frac{x^\beta}{6\beta} + b_2\Big) - \frac{1}{3}. \tag{3.50}$$

Case 2.

$$\{c = 2/9, k = -1, b_3 = -1/3, w_{1u} = w_{t1} = w_{x2} = -1/6, w_{2u} = w_{t2} = w_{x1} = 1/6\}. \tag{3.51}$$

In this case, Eq (3.46) can be written as the following special form of the fractional Burgers-Huxley equation:

$$D_t^{\alpha}u - 3u \cdot D_x^{\beta}u + D_x^{2\beta}u + \frac{2}{9}u + u^2 + u^3 = 0. \tag{3.52}$$

The hyperbolic function solutions to Eq (3.52) which correspond to this set of parameters is as follows:

$$u(x,t) = -\frac{1}{6}\tanh\Big(-\frac{t^{\alpha}}{6\alpha} + \frac{x^{\beta}}{6\beta} + b_1\Big) + \frac{1}{6}\coth\Big(\frac{t^{\alpha}}{6\alpha} - \frac{x^{\beta}}{6\beta} + b_2\Big) - \frac{1}{3}. \tag{3.53}$$

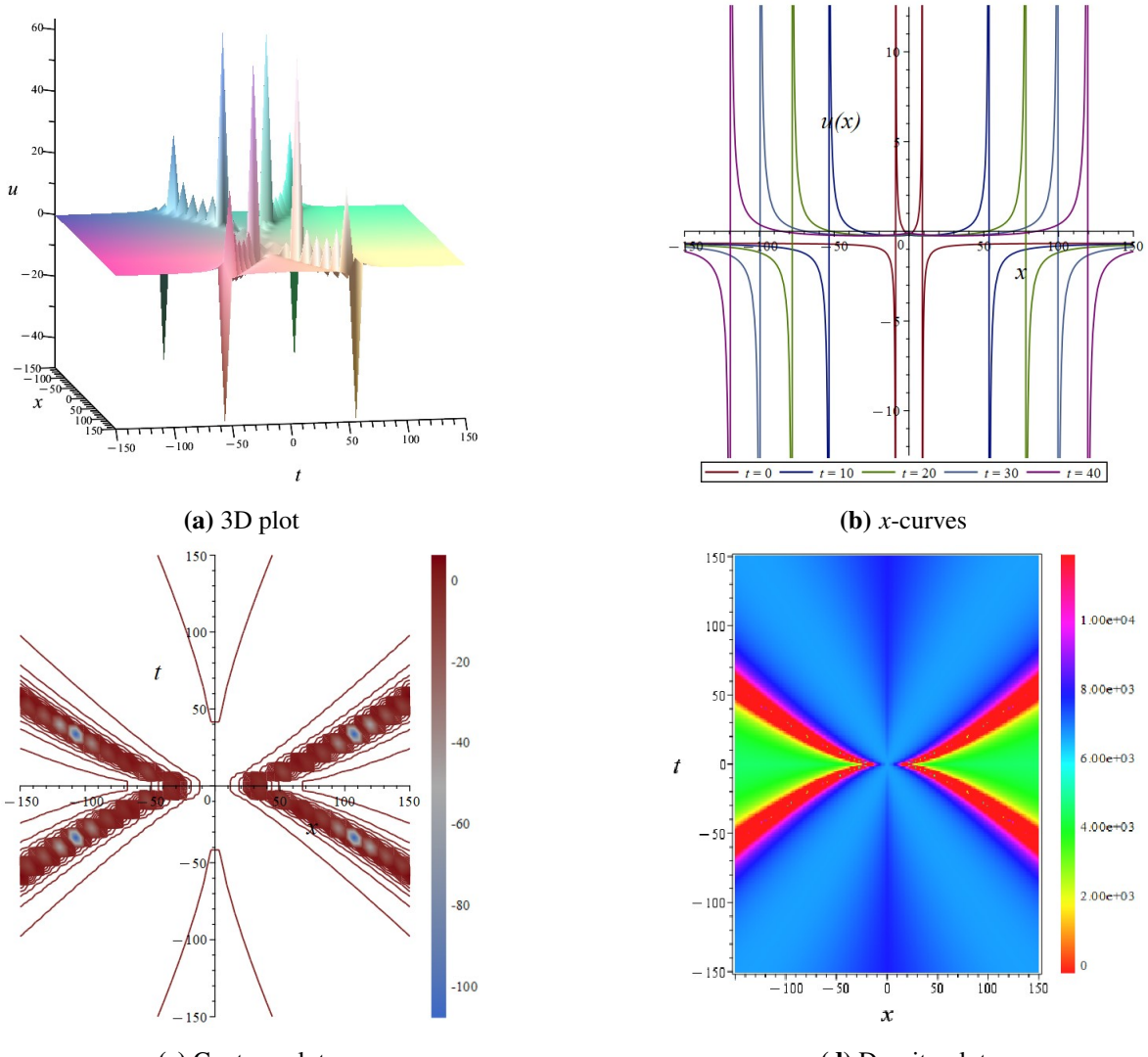

(a) 3D plot

(b) x-curves

(c) Contour plot

(d) Density plot

Figure 5. The 3D plot, curves plot, contour plot, and density plot of the solution Eq (3.53).

With the parameters $b_1 = 1$ and $b_2 = 1$ in Eq (3.53), and the fractional orders set to $\alpha = 0.4$ and $\beta = 0.4$, the dynamical characteristics of the fractional Burgers-Huxley equation are clearly revealed. The three-dimensional visualization of the solution over the space-time domain $[-150, 150] \times [-150, 150]$ is presented in Figure 5(a). Correspondingly, Figure 5(b) displays the spatial profile of the solution for $t \in [-150, 150]$, thus providing insight into its local behavior. Finally, the contour plot and density plot of the solution are illustrated in Figure 5(c),(d), respectively. Figure 5 comprehensively depicts the unique spatiotemporal evolution of an analytical solution to the fractional Burgers-Huxley equation through four types of subplots. The 3D surface plot illustrates a complex waveform structure formed under the combined modulation of nonlinear convection, fractional-order diffusion, and a polynomial reaction source term, thereby exhibiting features such as wave steepening, local oscillations, or waveform distortion. The 2D curve graph clearly shows the spatial distribution of the solution at specific instants, with its profile revealing the dynamic balance between nonlinear steepening and the stabilizing effect introduced by the reaction term. On the spatiotemporal plane, the contour plot marks the core propagation path and velocity variation of the wave peak with dense ring-like or band-shaped distributions, while the density map visually reflects, through color intensity and diffusion patterns, the complex physical process of how system energy is aggregated by nonlinear terms, dissipated by fractional-order diffusion, and simultaneously excited or suppressed by the polynomial reaction source term during propagation. The overall image highlights the rich dynamical phenomena characteristic of this equation as a reaction-convection-diffusion model. This result confirms, both visually and mathematically, the theoretical value and application potential of the fractional Burgers-Huxley equation to describe physical-biological propagation processes characterized by memory effects, nonlinear steepening, and self-regulating mechanisms, such as neural impulse transmission and the dynamics of reaction fronts in chemical systems.

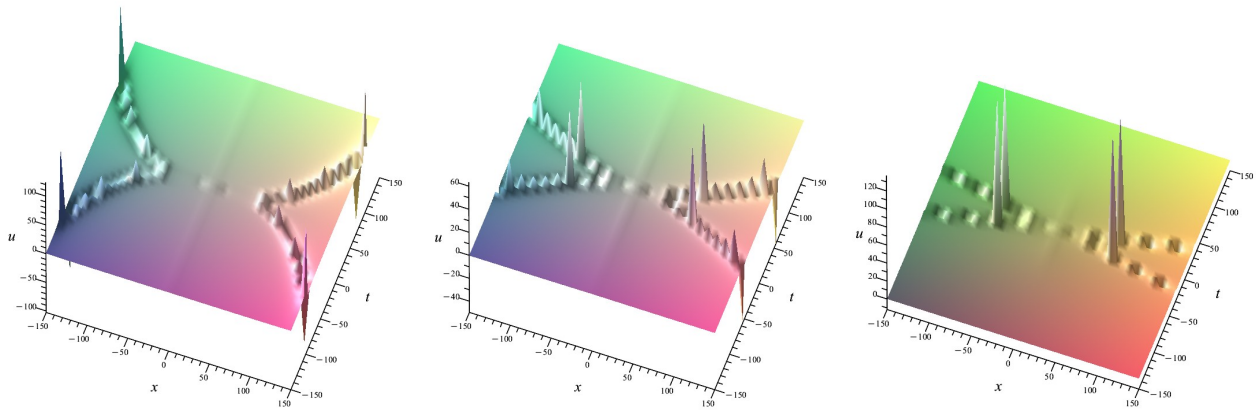

(a) $\alpha = 0.2, \beta = 0.4$ **(b)** $\alpha = 0.4, \beta = 0.4$ **(c)** $\alpha = 0.6, \beta = 0.4$

Figure 6. The 3D plots of the solution Eq (3.53) at different fractional derivative values.

Figure 6 visually illustrates the three-dimensional waveform evolution of the analytical solution Eq (3.53) to the Eq (3.46) under different fractional derivative values.Under different combinations of values for the fractional derivative orders α and β, the solution of Eq (3.53) exhibits distinct waveform evolution characteristics. As the value of α increases(e.g., from 0.2 to 0.6), the time evolution behavior of the system tends to become smoother, with enhanced diffusion or dissipation effects in the

temporal dimension. The steepness of the waveform decreases along the time direction, thus demonstrating stronger memory or delay effects. Meanwhile, with β fixed at 0.4, the non-locality of the spatial fractional derivative leads to a certain degree of structural stability in the spatial distribution of the waveform. However, changes in α significantly modulate the temporal dynamic behavior. Overall, the fractional parameters α and β jointly regulate the decay rate, waveform steepness, and structural preservation capability of the solution, thus reflecting the critical role of fractional calculus in describing physical processes with memory and non-local characteristics.

3.2.2. Exponential function interactive solutions

By the same discussion as Subsection 3.1.2, various exponential function interactive solutions of Eq (3.46) are obtained in the sequel.

Case 1. 2-2-2-1 model

Case 1.1

$$\begin{aligned}&\Big\{c=-(w_{13}^2w_{3u}^2w_{4u}^2+2b_5w_{13}w_{14}w_{3u}w_{4u}+b_5^2w_{14}^2+w_{13}w_{14}w_{3u}w_{4u}+b_5w_{14}^2)/w_{14}^2,\\&k=3w_{14}(w_{13}w_{3u}w_{4u}w_{x1}-w_{13}w_{3u}w_{4u}w_{x2}+b_5w_{14}w_{x1}-b_5w_{14}w_{x2})/(w_{13}^2w_{3u}^2w_{4u}^2\\&+2b_5w_{13}w_{14}w_{3u}w_{4u}+b_5^2w_{14}^2+2w_{14}^2w_{x1}^2-4w_{14}^2w_{x1}w_{x2}+2w_{14}^2w_{x2}^2),b_3=0,b_4=0,\\&b_5=b_5,w_{13}=w_{13},w_{14}=w_{14},w_{23}=-b_5w_{24}/(w_{3u}w_{4u}),w_{24}=w_{24},w_{3u}=w_{3u},\\&w_{4u}=w_{4u},w_{t1}=(w_{13}^2w_{3u}^2w_{4u}^2+2b_5w_{13}w_{14}w_{3u}w_{4u}+b_5^2w_{14}^2+w_{13}w_{14}w_{3u}w_{4u}-w_{14}^2w_{x1}^2\\&+2w_{14}^2w_{x1}w_{x2}-w_{14}^2w_{x2}^2+b_5w_{14}^2+w_{14}^2w_{t2})/w_{14}^2,w_{t2}=w_{t2},w_{x1}=w_{x1},w_{x2}=w_{x2}\Big\}.\end{aligned}\tag{3.54}$$

$$u(x,t)=\frac{(w_{13}w_{3u}w_{4u}+b_5w_{14})\mathrm{e}^{Tw_{t1}+Xw_{x1}+b_1}}{w_{14}\mathrm{e}^{Tw_{t1}+Xw_{x1}+b_1}+w_{24}\mathrm{e}^{Tw_{t2}+Xw_{x2}+b_2}},\tag{3.55}$$

where $T=t^\alpha/\alpha$, $X=x^\beta/\beta$, and w_{t1} is indicated in Eq (3.54).

Case 1.2

$$\begin{aligned}&\Big\{c=-(w_{13}^2w_{3u}^2w_{4u}^2+2b_5w_{13}w_{14}w_{3u}w_{4u}+b_5^2w_{14}^2+w_{13}w_{14}w_{3u}w_{4u}+b_5w_{14}^2)/w_{14}^2,\\&k=3w_{14}(2w_{13}w_{3u}w_{4u}w_{x1}-2w_{13}w_{3u}w_{4u}w_{x2}+2b_5w_{14}w_{x1}-2b_5w_{14}w_{x2}+w_{14}w_{x1}-w_{14}w_{x2})\\&/(4w_{13}^2w_{3u}^2w_{4u}^2+8b_5w_{13}w_{14}w_{3u}w_{4u}+4b_5^2w_{14}^2+4w_{13}w_{14}w_{3u}w_{4u}+2w_{14}^2w_{x1}^2-4w_{14}^2w_{x1}w_{x2}\\&+2w_{14}^2w_{x2}^2+4b_5w_{14}^2+w_{14}^2),b_3=0,b_4=0,b_5=b_5,w_{13}=w_{13},w_{14}=w_{14},w_{23}=-w_{24}\\&\times(w_{13}w_{3u}w_{4u}+2b_5w_{14}+w_{14})/(w_{14}w_{3u}w_{4u}),w_{24}=w_{24},w_{3u}=w_{3u},w_{4u}=w_{4u},w_{t1}=\\&(2w_{13}w_{3u}w_{4u}w_{t2}+2b_5w_{14}w_{t2}+w_{14}w_{x1}^2-2w_{14}w_{x1}w_{x2}+w_{14}w_{x2}^2+w_{14}w_{t2})/(2w_{13}w_{3u}w_{4u}\\&+2b_5w_{14}+w_{14}),w_{t2}=w_{t2},w_{x1}=w_{x1},w_{x2}=w_{x2}\Big\}.\end{aligned}\tag{3.56}$$

$$u(x,t)=\frac{w_{3u}w_{4u}(w_{13}\mathrm{e}^{Tw_{t1}+xw_{x1}+b_1}+w_{23}\mathrm{e}^{Tw_{t2}+xw_{x2}+b_2})}{w_{14}\mathrm{e}^{Tw_{t1}+xw_{x1}+b_1}+w_{24}\mathrm{e}^{Tw_{t2}+xw_{x2}+b_2}}+b_5,\tag{3.57}$$

where $T=t^\alpha/\alpha$, $X=x^\beta/\beta$, and w_{t1}, w_{23} are indicated in Eq (3.56).

Case 1.3

$$\begin{cases} c = -(w_{23}^2 w_{3u}^2 w_{4u}^2 + 2b_5 w_{23} w_{24} w_{3u} w_{4u} + w_{24}^2 b_5^2 + w_{23} w_{24} w_{3u} w_{4u} + b_5 w_{24}^2)/w_{24}^2, \\ k = -3w_{24}(w_{23} w_{3u} w_{4u} w_{x1} - w_{23} w_{3u} w_{4u} w_{x2} + b_5 w_{24} w_{x1} - b_5 w_{24} w_{x2})/(w_{23}^2 w_{3u}^2 w_{4u}^2 \\ +2b_5 w_{23} w_{24} w_{3u} w_{4u} + b_5^2 w_{24}^2 + 2w_{24}^2 w_{x1}^2 - 4w_{24}^2 w_{x1} w_{x2} + 2w_{24}^2 w_{x2}^2), b_3 = 0, b_4 = 0, \\ b_5 = b_5, w_{13} = -b_5 w_{14}/(w_{3u} w_{4u}), w_{14} = w_{14}, w_{23} = w_{23}, w_{24} = w_{24}, w_{3u} = w_{3u}, w_{4u} = w_{4u}, \\ w_{t1} = -(w_{23}^2 w_{3u}^2 w_{4u}^2 + 2b_5 w_{23} w_{24} w_{3u} w_{4u} + b_5^2 w_{24}^2 + w_{23} w_{24} w_{3u} w_{4u} - w_{24}^2 w_{x1}^2 \\ +2w_{24}^2 w_{x1} w_{x2} - w_{24}^2 w_{x2}^2 + b_5 w_{24}^2 - w_{24}^2 w_{t2})/w_{24}^2, w_{t2} = w_{t2}, w_{x1} = w_{x1}, w_{x2} = w_{x2} \end{cases}. \tag{3.58}$$

$$u(x,t) = \frac{(w_{23} w_{3u} w_{4u} + b_5 w_{24}) e^{T w_{t2} + X w_{x2} + b_2}}{w_{14} e^{T w_{t1} + X w_{x1} + b_1} + w_{24} e^{T w_{t2} + X w_{x2} + b_2}}, \tag{3.59}$$

where $T = t^\alpha/\alpha$, $X = x^\beta/\beta$, and w_{t1} is denoted by Eq (3.58).

Case 2. 2-1-2-1 model

Case 2.1

$$\begin{cases} c = -(b_3^2 w_{3u}^2 w_{4u}^2 + 2b_3 b_4 b_5 w_{3u} w_{4u} + b_3 b_4 w_{3u} w_{4u} + b_4^2 b_5^2 + b_4^2 b_5)/b_4^2, w_{x1} = w_{x1}, \\ k = -3b_4 w_{x2}(b_3 w_{3u} w_{4u} + b_4 b_5)/(b_3^2 w_{3u}^2 w_{4u}^2 + 2b_3 b_4 b_5 w_{3u} w_{4u} + b_4^2 b_5^2 + 2b_4^2 w_{x2}^2), \\ b_3 = b_3, b_4 = b_4, b_5 = b_5, w_{13} = 0, w_{14} = 0, w_{23} = -b_5 w_{24}/(w_{3u} w_{4u}), w_{24} = w_{24}, \\ w_{3u} = w_{3u}, w_{4u} = w_{4u}, w_{t1} = w_{t1}, w_{t2} = -(b_3^2 w_{3u}^2 w_{4u}^2 + 2b_3 b_4 b_5 w_{3u} w_{4u} + b_4^2 b_5^2 \\ +b_3 b_4 w_{3u} w_{4u} - b_4^2 w_{x2}^2 + b_4^2 b_5)/b_4^2, w_{x2} = w_{x2} \end{cases}. \tag{3.60}$$

$$u(x,t) = \frac{b_3 w_{3u} w_{4u} + b_4 b_5}{w_{24} e^{T w_{t2} + x w_{x2} + b_2} + b_4}, \tag{3.61}$$

where $T = t^\alpha/\alpha$, $X = x^\beta/\beta$, and w_{t2} is denoted by Eq (3.60).

Case 2.2

$$\begin{cases} c = -(w_{23}^2 w_{3u}^2 w_{4u}^2 + 2b_5 w_{23} w_{24} w_{3u} w_{4u} + w_{24}^2 b_5^2 + w_{23} w_{24} w_{3u} w_{4u} + b_5 w_{24}^2)/w_{24}^2, \\ k = 3w_{24} w_{x2}(w_{23} w_{3u} w_{4u} + b_5 w_{24})/(w_{23}^2 w_{3u}^2 w_{4u}^2 + 2b_5 w_{23} w_{24} w_{3u} w_{4u} + b_5^2 w_{24}^2 \\ +2w_{24}^2 w_{x2}^2), b_3 = -b_4 b_5/(w_{3u} w_{4u}), b_4 = b_4, b_5 = b_5, w_{13} = 0, w_{14} = 0, w_{23} = w_{23}, \\ w_{24} = w_{24}, w_{3u} = w_{3u}, w_{4u} = w_{4u}, w_{t1} = w_{t1}, w_{t2} = (w_{23}^2 w_{3u}^2 w_{4u}^2 + 2b_5 w_{23} w_{24} w_{3u} w_{4u} \\ +b_5^2 w_{24}^2 + w_{23} w_{24} w_{3u} w_{4u} - w_{24}^2 w_{x2}^2 + b_5 w_{24}^2)/w_{24}^2, w_{x1} = w_{x1}, w_{x2} = w_{x2} \end{cases}. \tag{3.62}$$

$$u(t,x) = \frac{(w_{23} w_{3u} w_{4u} + b_5 w_{24}) e^{T w_{t2} + X w_{x2} + b_2}}{w_{24} e^{T w_{t2} + X w_{x2} + b_2} + b_4}, \tag{3.63}$$

where $T = t^\alpha/\alpha$, $X = x^\beta/\beta$, and w_{t2} is denoted by Eq (3.62).

3.3. Fractional Kdv-Burgers equation

A third important example is the fractional Kdv-Burgers equation, which could be formulated as follows:

$$D_t^\alpha u + au \cdot D_x^\beta u - bD_x^{2\beta} u + cD_x^{3\beta} u = 0, \tag{3.64}$$

where $0 < \alpha, \beta \leq 1$, and a, b, c are arbitrary constants, and u is the function of (t, x). When $b = 0$, Eq (3.64) is reduced to the fractional Kdv equation. When $c = 0$, Eq (3.64) is reduced to the fractional Burgers equation.

For simplicity, only exponential function interactive solutions of fractional Kdv-Burgers equation are explored by the fractional variable transformation NN method.

By the same discussion as Subsections 3.1.2 and 3.2.2, some effective solutions are obtained. According to the way in which the NN connects, all efficient solutions of Eq (3.64) are classified into four cases as follows.

Case 1. 2-2-2-1 model

Case 1.1

$$\begin{aligned}&\{a = a, b = b, c = c, b_3 = 0, b_4 = 0, b_5 = b_5, w_{13} = w_{13}, w_{14} = w_{14}, w_{23} = w_{23}, w_{24} = w_{24},\\ &w_{3u} = w_{3u}, w_{4u} = w_{4u}, w_{t1} = w_{t2}, w_{t2} = w_{t2}, w_{x1} = w_{x2}, w_{x2} = w_{x2}\}.\end{aligned} \tag{3.65}$$

$$u(x,t) = \frac{w_{3u}w_{4u}\left(w_{13}\mathrm{e}^{Tw_{t2}+Xw_{x2}+b_1} + w_{23}\mathrm{e}^{Tw_{t2}+Xw_{x2}+b_2}\right)}{w_{14}\mathrm{e}^{Tw_{t2}+Xw_{x2}+b_1} + w_{24}\mathrm{e}^{Tw_{t2}+Xw_{x2}+b_2}} + b_5, \tag{3.66}$$

where $T = t^\alpha/\alpha$, and $X = x^\beta/\beta$.

Case 1.2

$$\begin{aligned}&\{a = 0, b = b, c = c, b_3 = b_4 = 0, b_5 = b_5, w_{13} = w_{13}, w_{14} = 0, w_{23} = w_{23}, w_{24} = w_{24},\\ &w_{t1} = -cw_{x1}^3 + 3cw_{x1}^2w_{x2} - 3cw_{x1}w_{x2}^2 + cw_{x2}^3 + bw_{x1}^2 - 2bw_{x1}w_{x2} + bw_{x2}^2 + w_{t2},\\ &w_{3u} = w_{3u}, w_{4u} = w_{4u}, w_{t2} = w_{t2}, w_{x1} = w_{x1}, w_{x2} = w_{x2}\}.\end{aligned} \tag{3.67}$$

$$u(x,t) = \frac{w_{4u}w_{3u}w_{13}\mathrm{e}^{(w_{x1}-w_{x2})^2(-cw_{x1}+cw_{x2}+b)T+X(w_{x1}-w_{x2})+b_1-b_2} + w_{4u}w_{3u}w_{23} + b_5w_{24}}{w_{24}}, \tag{3.68}$$

where $T = t^\alpha/\alpha$, and $X = x^\beta/\beta$.

Case 1.3

$$\begin{aligned}&\{a = 0, b = b, c = c, b_3 = b_3, b_4 = 0, b_5 = b_5, w_{13} = w_{13}, w_{14} = 0, w_{23} = w_{23}, w_{24} = w_{24},\\ &w_{3u} = w_{3u}, w_{4u} = w_{4u}, w_{t1} = -cw_{x1}^3 + 3cw_{x1}^2w_{x2} - 3cw_{x1}w_{x2}^2 + bw_{x1}^2 - 2bw_{x1}w_{x2},\\ &w_{t2} = -cw_{x2}^3 - bw_{x2}^2, w_{x1} = w_{x1}, w_{x2} = w_{x2}\Big\}.\end{aligned} \tag{3.69}$$

$$u(x,t) = \frac{w_{4u}w_{3u}w_{13}\mathrm{e}^{a_1T+X(w_{x1}-w_{x2})+b_1-b_2} + w_{4u}w_{3u}w_{23} + \mathrm{e}^{T(cw_{x2}^3+bw_{x2}^2)-Xw_{x2}-b_2}b_3w_{3u}w_{4u}}{w_{24}} + b_5, \tag{3.70}$$

where $T = t^\alpha/\alpha$, $X = x^\beta/\beta$, and $a_1 = (w_{x1} - w_{x2})^2(-cw_{x1} + cw_{x2} + b)$.

Case 2. 2-1-2-1 model

Case 2.1

$$\begin{aligned}&\{a=0,b=b,c=c,b_3=b_3,b_4=0,b_5=b_5,w_{13}=w_{14}=0,w_{23}=w_{23},w_{24}=w_{24},\\&w_{3u}=w_{3u},w_{4u}=w_{4u},w_{t1}=w_{t1},w_{t2}=-cw_{x2}^3-bw_{x2}^2,w_{x1}=w_{x1},w_{x2}=w_{x2}\Big\}.\end{aligned} \tag{3.71}$$

$$u(x,t)=\frac{b_3w_{3u}w_{4u}\mathrm{e}^{T\left(cw_{x2}^3+bw_{x2}^2\right)-Xw_{x2}-b_2+w_{4u}w_{3u}w_{23}}}{w_{24}}+b_5, \tag{3.72}$$

where $T=t^\alpha/\alpha$, and $X=x^\beta/\beta$.

Case 3. 2-2-1-1 model

Case 3.1

$$\begin{aligned}&\{a=0,b=b,c=c,b_3=b_3,b_4=b_4,b_5=b_5,w_{13}=w_{13},w_{14}=0,w_{23}=w_{23},w_{24}=0,\\&w_{3u}=w_{3u},w_{4u}=w_{4u},w_{t1}=-cw_{x1}^3+bw_{x1}^2,w_{t2}=-cw_{x2}^3+bw_{x2}^2,w_{x1}=w_{x1},w_{x2}=w_{x2}\Big\}.\end{aligned} \tag{3.73}$$

$$u(x,t)=\frac{w_{3u}w_{4u}\Big(w_{13}\mathrm{e}^{T(bw_{x1}^2-cw_{x1}^3)+Xw_{x1}+b_1}+w_{23}\mathrm{e}^{T(bw_{x2}^2-cw_{x2}^3)+Xw_{x2}+b_2}+b_3\Big)}{b_4}+b_5, \tag{3.74}$$

where $T=t^\alpha/\alpha$, and $X=x^\beta/\beta$.

The dynamical features of the fractional Kdv-Burgers equation under the parameter configuration specified in Eq (3.74) ($b=2,c=1,b_1=1,b_2=1,b_3=1,b_4=1,b_5=1,w_{x1}=1,w_{x2}=1,w_{13}=1,w_{23}=1,w_{3u}=1,w_{4u}=1,\alpha=0.5,\beta=0.5$) are depicted in Figure 7. The solution is represented in a 3D diagram over $[0,5]\times[0,5]$ in Figure 7(a). Its local behavior is analyzed using the spatial curve plotted for $t\in[0,5]$ in Figure 7(b), while Figure 7(c),(d) present the contour and density plots, respectively. From a mathematical visualization standpoint, the solution to this fractional KdV-Burgers equation manifests as a smooth and monotonically increasing three-dimensional surface. It uniformly rises along the diagonal direction on the *x*-*t* plane, devoid of oscillations or abrupt structural changes. The contour lines exhibit an outward-expanding arc-like distribution, while the density plot reveals a smooth transition in amplitude from the upper left to the lower right. Overall, the visual characteristics suggest a pattern of uniform diffusion. This solution mathematically verifies the smooth diffusion behavior of the fractional Kdv-Burgers equation under dissipation dominance. It reveals a typical pattern of wave suppression and energy dissipation in nonlocal media with memory effects, thus providing a theoretical paradigm to understand the nonclassical transport processes in complex media.

Figure 8 visually illustrates the three-dimensional waveform evolution of the analytical solution Eq (3.74) to the Eq (3.64) under different fractional derivative values. From the figure, it can be observed that as the fractional derivative varies, and the shape of the solution remains unchanged, while the solution exhibits an exponential growth trend over time and space. However, when the fractional derivative changes, both the peak amplitude and the growth rate of the solution undergo noticeable changes.

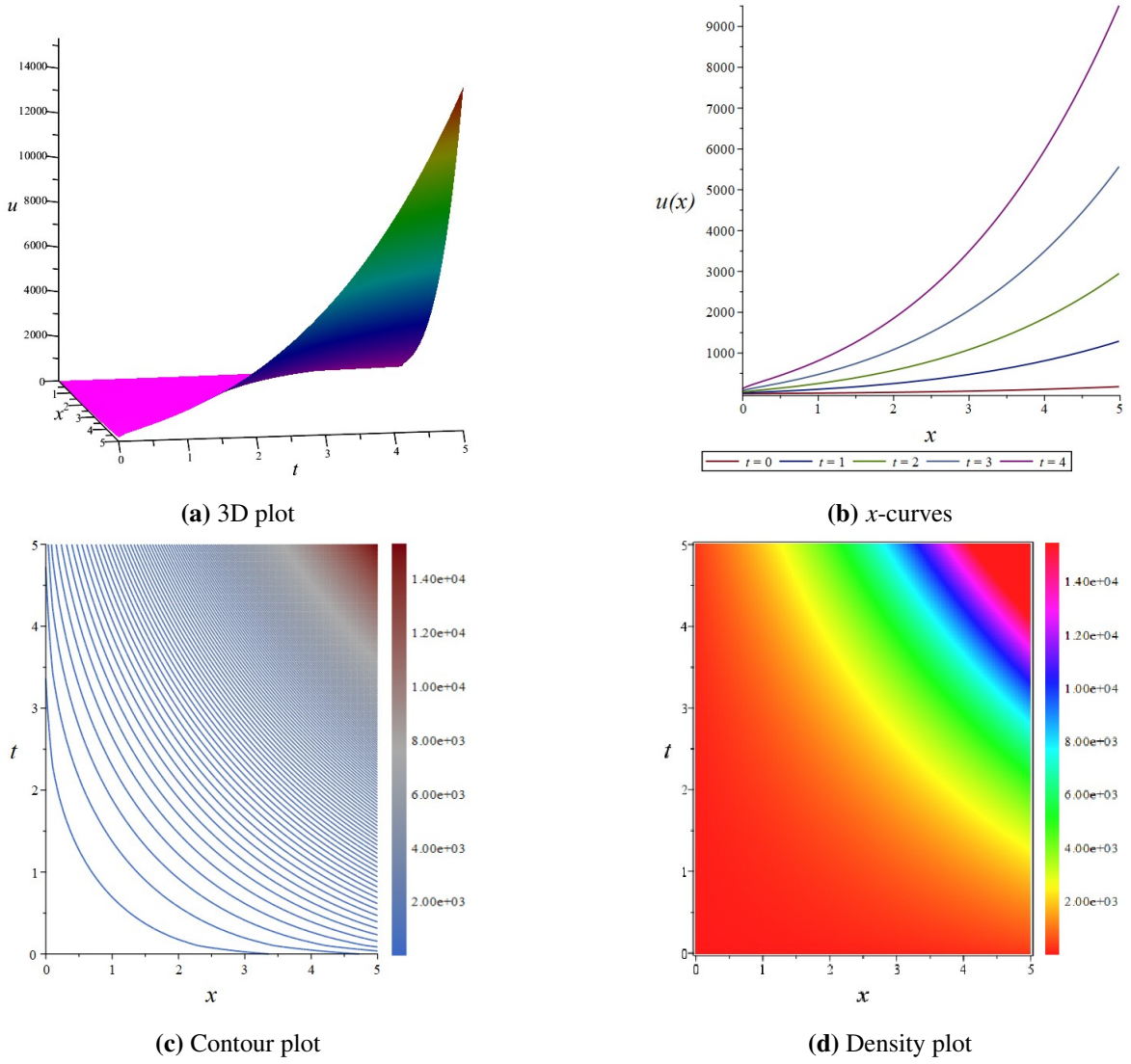

(a) 3D plot **(b)** x-curves

(c) Contour plot **(d)** Density plot

Figure 7. The 3D plot, curves plot, contour plot, and density plot of the solution Eq (3.74).

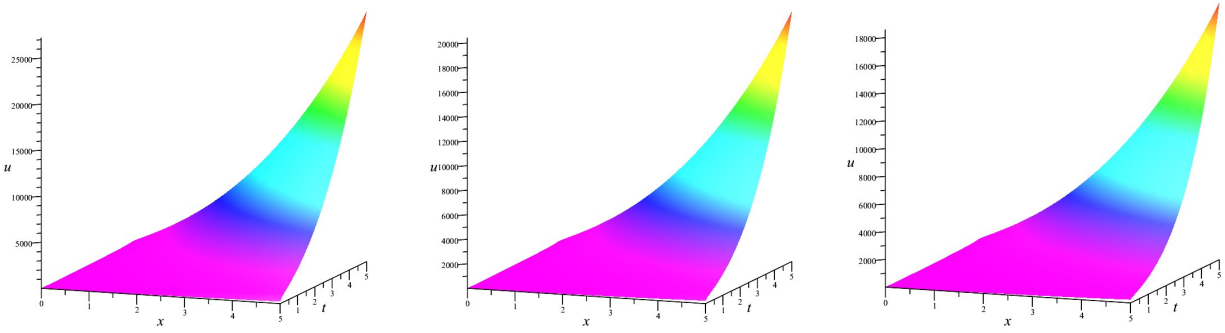

(a) $\alpha = 0.4, \beta = 0.4$ **(b)** $\alpha = 0.5, \beta = 0.4$ **(c)** $\alpha = 0.6, \beta = 0.4$

Figure 8. The 3D plots of the solution Eq (3.74) at different fractional derivative values.

Case 4. 2-1-1-1 model

Case 4.1

$$\begin{aligned}&\{a=0, b=b, c=c, b_3=b_3, b_4=b_4, b_5=b_5, w_{13}=w_{13}, w_{14}=w_{14}, w_{23}=w_{23}, w_{24}=0,\\ &w_{3u}=w_{3u}, w_{4u}=w_{4u}, w_{t1}=0, w_{t2}=-cw_{x2}^3+bw_{x2}^2, w_{x1}=0, w_{x2}=w_{x2}\Big\}.\end{aligned} \tag{3.75}$$

$$u(x,t)=\frac{w_{3u}w_{4u}\Big(w_{23}\mathrm{e}^{T(bw_{x2}^2-cw_{x2}^3)+Xw_{x2}+b_2}+w_{13}\mathrm{e}^{b_1}+b_3\Big)}{w_{14}\mathrm{e}^{b_1}+b_4}+b_5, \tag{3.76}$$

where $T=t^\alpha/\alpha$, and $X=x^\beta/\beta$.

Remark 1. *All the solutions obtained in the present paper for Eqs (3.1), (3.46), and (3.64) to understand the checked by thg Maple software. Substituting the obtained result into the original equation shows that both sides are equal.*

Remark 2. *We only consider two special cases solutions of Eqs (3.1), (3.46), and (3.64). If we take the activation function as other elementary functions such as* $\sin(\cdot)$, $\cos(\cdot)$, $\mathrm{sech}(\cdot)$, *and* $\ln(\cdot)$, *we can get obtain additional solutions for Eqs (3.1), (3.46), (3.64), and many other nonlinear space-time fPDEs.*

Remark 3. *In this paper, we only consider NNs that contain two hidden layers, where each hidden layer has two neurons. If we consider a NN with more than two hidden layers, where each hidden layer has more than two neurons, then we may obtain more complex solutions of Eqs (3.1), (3.46), (3.64), and many other nonlinear space-time fPDEs.*

4. Conclusions

First, the fractional variable transformation NN method was applied to find analytical solutions of nonlinear space-time fPDEs. To our best knowledge, the solutions for Eqs (3.1), (3.46), and (3.64) obtained in this paper have not seen previous studies. In fact, the solutions obtained by this method can be degenerated into the traveling wave solutions of the problems under consideration when the fractional derivatives $\alpha=\beta=1$. Therefore, the method presented in this paper can be regarded as an extension formula of the NN method under the fractional derivative situation. It is worth mentioning that the method can be designed together with some explicit formula solutions, such as triangular periodic solutions, rational function solutions, or exponential function interactive solutions, and so on, and many other exact solutions of nonlinear space-time fPDEs may be obtained by similar ways. In summary, we have shown that the fractional variable transformation neural networks method is quite effective in handling fPDEs and can also be extended to solve other fPDEs.

Since PINNs are data-driven models, they require a substantial number of data samples, which leads to high computational time costs. Compared to PINNs, the method proposed in this paper does not require data samples to obtain the exact analytical solution of the equation and is free from approximation errors. The fVTNNs method solely leverages the NNs structure to construct potential analytical solutions, without incorporating the training mechanism of NNs, thus eliminating the need for optimization algorithms. Furthermore, the proposed method is highly flexible and can be tailored to address a wide range of nonlinear space-time fPDEs through the adjustment of its NN parameters.

In the future work, we aim to extend this type of NN-based analytical method to solving other complex equations and high-dimensional problems [44–46], to cope with more challenging scientific

computing scenarios [47–49]. Furthermore, we will extend the proposed fVTNNs to solve nonlinear fPDEs in other senses, such as the normalized fractional derivative [50, 51].

Use of AI tools declaration

The authors declare they have not used Artificial Intelligence (AI) tools in the creation of this article.

Authors contributions

Limei Yan and Yanqin Liu: Conceptualization, Methodology; Shanhao Yuan, Runfa Zhang, and Qiuping Li: Software, Visualization, Validation; Limei Yan and Shanhao Yuan: Writing-Original draft preparation; Yanqin Liu: Writing-Reviewing & editing. All authors have read and approved the final version of the manuscript for publication.

Acknowledgements

This article is supported the Natural Science Foundation of Shandong Province (Grant No. ZR2023MA062), the Belt and Road Special Foundation of the State Key Laboratory of Water Disaster Prevention (Grant No. 2023491911), Tianyuan Fund for Mathematics of the National Natural Science Foundation of China (Grant No. 12426105), and the Scientific and Technological Innovation Programs (STIP) of Higher Education Institutions in Shanxi (Grant No. 2024L022).

Conflict of interest

The authors declare there are no conflicts of interest.

References

1. J. Sabatier, O. P. Agrawal, J. A. T. Machado, *Advances in Fractional Calculus: Theoretical Developments and Applications in Physics and Engineering*, Springer, 2007. https://doi.org/10.1007/978-1-4020-6042-7
2. D. Baleanu, K. Diethelm, E. Scalas, J. J. Trujillo, *Fractional Calculus Models and Numerical Methods*, World Scientific, 2012. https://doi.org/10.1142/8180
3. X. Y. Guo, Z. W. Fu, An initial and boundary value problem of fractional Jeffreys' fluid in a porous half space, *Comput. Math. Appl.*, **78** (2019), 1801–1810. https://doi.org/10.1016/j.camwa.2015.11.020
4. J. H. Ma, Y. Q. Liu, Exact solutions for a generalized nonlinear fractional Fokker-Planck equation, *Nonlinear Anal. Real World Appl.*, **11** (2010), 515–521. https://doi.org/10.1016/j.nonrwa.2009.01.006
5. T. M. Elzaki, M. Z. Mohamed, A novel analytical method for the exact solution of the fractional-order biological population model, *Acta Mech. Autom.*, **18** (2024), 564–570. https://doi.org/10.2478/ama-2024-0059

6. Z. H. Liu, Y. Z. Ding, C. W. Liu, C. Y. Zhao , Existence and uniqueness of solutions for singular fractional differential equation boundary value problem with p-Laplacian, *Adv. Differ. Equ.*, **2020** (2020), 83. https://doi.org/10.1186/s13662-019-2482-9

7. Y. M. Zi, Y. Wang, Positive solutions for Caputo fractional differential system with coupled boundary conditions, *Adv. Differ. Equ.*, **2019** (2019), 80. https://doi.org/10.1186/s13662-019-2016-5

8. S. H. Yuan, Y. Q. Liu, Y. B. Xu, Q. P. Li, C. Guo, Y. F. Shen, Gradient-enhanced fractional physics-informed neural networks for solving forward and inverse problems of the multiterm time-fractional Burger-type equation, *AIMS Math.*, **9** (2024), 27418–27437. https://doi.org/10.3934/math.20241332

9. X. Y. Jiang, M. Y. Xu, The time-fractional heat conduction equation in the general rthogonal curvilinear coordinate and the cylindrical coordinate systems, *Physica A*, **389** (2010), 3368–3374. https://doi.org/10.1016/j.physa.2010.04.023

10. X. Y. Jiang, H. T. Qi, M. Y. Xu, Exact solutions of fractional Schrödinger-like equation with a nonlocal term, *J. Math. Phys.*, **52** (2011), 042105. https://doi.org/10.1063/1.3576189

11. X. C. Li, M. Y. Xu, X. Y. Jiang, Homotopy perturbation method to time-fractional diffusion equation with a moving boundary condition, *Appl. Math. Comput.*, **208** (2009), 434–439. https://doi.org/10.1016/j.amc.2008.12.023

12. Y. B. Xu, Y. Q. Liu, X. L. Yin, L. B. Feng, Z. H. Wang, A compact scheme combining the fast time stepping method for solving 2D fractional subdiffusion equations, *Fractal Fract.*, **7** (2023), 186. https://doi.org/10.3390/fractalfract7020186

13. T. Y. Liu, H. X. Zhang, S. Wang, A new high-order compact CN-ADI scheme on graded meshes for three-dimensional nonlinear PIDEs with multiple weakly singular kernels, *Appl. Math. Lett.*, **171** (2025), 109697. https://doi.org/10.1016/j.aml.2025.109697

14. Z. Y. Chen, H. X. Zhang, H. Chen, ADI compact difference scheme for the two-dimensional integro-differential equation with two fractional Riemann–Liouville integral kernels, *Fractal Fract.*, **8** (2024), 707. https://doi.org/10.3390/fractalfract8120707

15. J. X. Zhang, X. H. Yang, S. Wang, The ADI difference and extrapolation scheme for high-dimensional variable coefficient evolution equations, *Electron. Res. Arch.*, **33** (2025), 3305–3327. https://doi.org/10.3934/era.2025146

16. A. J. Hussein, A weak Galerkin finite element method for solving time-fractional coupled Burgers' equations in two dimensions, *Appl. Numer. Math.*, **156** (2020), 265–275. https://doi.org/10.1016/j.apnum.2020.04.016

17. H. Liu, X. C. Zheng, C. J. Chen, H. Wang, A characteristic finite element method for the time-fractional mobile/immobile advection diffusion model, *Adv. Comput. Math.*, **47** (2021), 41. https://doi.org/10.1007/s10444-021-09867-6

18. B. L. Yin, Y. Liu, H. Li, F. H. Zeng, A class of efficient time-stepping methods for multi-term time-fractional reaction-diffusion-wave equations, *Appl. Numer. Math.*, **165** (2021), 56–82. https://doi.org/10.1016/j.apnum.2021.02.007

19. C. Han, X. Lü, H. Tian, Long-time diffusion behavior of variable-coefficient fractional reaction–diffusion model for pattern dynamics, *Commun. Nonlinear Sci. Numer. Simul.*, **151** (2025), 109082. https://doi.org/10.1016/j.cnsns.2025.109082

20. Y. Q. Liu, H. G. Sun, X. L. Yin, L. B. Feng, Fully discrete spectral method for solving a novel multi-term time-fractional mixed diffusion and diffusion-wave equation, *Z. Angew. Math. Phys.*, **71** (2020), 21. https://doi.org/10.1007/s00033-019-1244-6

21. Y. Q. Liu, X. L. Yin, F. W. Liu, X. Y. Xin, Y. F. Shen, L. B. Feng, An alternating direction implicit legendre spectral method for simulating a 2D multi-term time-fractional oldroyd-b fluid type diffusion equation, *Comput. Math. Appl.*, **113** (2022), 160–173. https://doi.org/10.1016/j.camwa.2022.03.020

22. Y. B. Xu, Y. Q. Liu, X. L. Yin, L. B. Feng, Z. H. Wang, Q. P. Li, A fast time stepping Legendre spectral method for solving fractional Cable equation with smooth and non-smooth solutions, *Math. Comput. Simul.*, **211** (2023), 154–170. https://doi.org/10.1016/j.matcom.2023.04.009

23. A. Yildirim, Application of the homotopy perturbation method for the Fokker-Planck equation, *Int. J. Numer. Methods Biomed. Eng.*, **26** (2010), 1144–1154. https://doi.org/10.1002/cnm.1200

24. H. Jafari, S. Seifi, Solving a system of nonlinear fractional partial differential equations using homotopy analysis method, *Commun. Nonlinear Sci. Numer. Simul.*, **14** (2009), 1962–1969. https://doi.org/10.1016/j.cnsns.2008.06.019

25. M. H. Taha, M. A. Ramadan, D. Baleanu, G. M. Moatimid, A novel analytical technique of the fractional Bagley-Torvik equations for motion of a rigid plate in Newtonian fluids, *Comput. Modell. Eng. Sci.*, **124** (2020), 969–983. https://doi.org/10.32604/cmes.2020.010942

26. S. T. Mohyud-Din, S. Bibi, Exact solutions for nonlinear fractional differential equations using (G'/G^2)-expansion method, *Alexandria Eng. J.*, **57** (2018), 1003–1008. https://doi.org/10.1016/j.aej.2017.01.035

27. S. Sirisubtawee, S. Koonprasert, S. Sungnul, T. Leekparn, Exact traveling wave solutions of the space-time fractional complex Ginzburg-Landau equation and the space-time fractional Phi-4 equation using reliable methods, *Adv. Differ. Equ.*, **2019** (2019), 219. https://doi.org/10.1186/s13662-019-2154-9

28. O. Guner, New travelling wave solutions for fractional regularized long-wave equation and fractional coupled Nizhnik-Novikon-Veselov equation, *Int. J. Optim. Control Theor. Appl.*, **8** (2018), 63–72. https://doi.org/10.11121/ijocta.01.2018.00417

29. P. Prakash, R. Sahadevan, Lie symmetry analysis and exact solution of certain fractional ordinary differential equations, *Nonlinear Dyn.*, **89** (2017), 305–319. https://doi.org/10.1007/s11071-017-3455-8

30. E. Saberi, S. R. Hejazi, Lie symmetry analysis, conservation laws and exact solutions of the time-fractional generalized Hirota–Satsuma coupled KdV system, *Physica A*, **492** (2018), 296–307. https://doi.org/10.1016/j.physa.2017.09.092

31. Z. Y. Zhang, G. F. Li, Lie symmetry analysis and exact solutions of the time-fractional biological population model, *Physica A*, **540** (2020), 123134. https://doi.org/10.1016/j.physa.2019.123134

32. L. H. Zhang, B. Shen, H. B. Jiao, G. W. Wang, Z. L. Wang, Exact solutions for the KMM system in (2+1)-dimensions and its fractional form with beta-derivative, *Fractal Fract.*, **6** (2022), 520. https://doi.org/10.3390/fractalfract6090520

33. A. M. El-Sayed, S. Z. Rida, A. A. Arafa, Exact solutions of fractional-order biological population model, *Commun. Theor. Phys.*, **52** (2009), 992–996. https://doi.org/10.1088/0253-6102/52/6/04

34. X. Peng, Y. W. Zhao, X. Lü, Data-driven solitons and parameter discovery to the (2 + 1)-dimensional NLSE in optical fiber communications, *Nonlinear Dyn.*, **112** (2024), 1291–1306. https://doi.org/10.1007/s11071-023-09083-5

35. Y. B. Su, X. Lü, S. K. Li, L. X. Yang, Z. Y. Gao, Self-adaptive equation embedded neural networks for traffic flow state estimation with sparse data, *Phys. Fluids*, **36** (2024), 104127. https://doi.org/10.1063/5.0230757

36. Y. Zhang, X. Lü, Data-driven solutions and parameter discovery of the extended higher-order nonlinear Schrödinger equation in optical fibers, *Physica D*, **468** (2024), 134284. https://doi.org/10.1016/j.physd.2024.134284

37. M. H. Guo, X. Lü, Y. X. Jin, Extraction and reconstruction of variable-coefficient governing equations using Res-KAN integrating sparse regression, *Physica D*, **481** (2025), 134689. https://doi.org/10.1016/j.physd.2025.134689

38. R. F. Zhang, M. C. Li, A. Cherraf, S. R. Vadyala, The interference wave and the bright and dark soliton for two integro-differential equation by using BNNM, *Nonlinear Dyn.*, **111** (2023), 8637–8646. https://doi.org/10.1007/s11071-023-08257-5

39. N. Lü, Y. C. Yue, R. F. Zhang, X. G. Yuan, R. Wang, Fission and annihilation phenomena of breather/rogue waves and interaction phenomena on nonconstant backgrounds for two KP equations, *Nonlinear Dyn.*, **111** (2023), 10357–10366. https://doi.org/10.1007/s11071-023-08329-6

40. Y. Zhang, R. F. Zhang, K. V. Yuen, Neural network-based analytical solver for Fokker-Planck equation, *Eng. Appl. Artif. Intell.*, **125** (2023), 106721. https://doi.org/10.1016/j.engappai.2023.106721

41. R. Khalil, M. Al Horani, A. Yousef, M. Sababheh, A new definition of fractional derivative, *J. Comput. Appl. Math.*, **264** (2014), 65–70. https://doi.org/10.1016/j.cam.2014.01.002

42. T. Abdeljawad, On conformable fractional calculus, *J. Comput. Appl. Math.*, **279** (2015), 57–66. https://doi.org/10.1016/j.cam.2014.10.016

43. A. A. Soliman, The modified extended tanh-function method for solving Burgers-type equations, *Physica A*, **361** (2006), 394–404. https://doi.org/10.1016/j.physa.2005.07.008

44. T. Y. Liu, H. X. Zhang, X. H. Yang, The BDF2-ADI compact difference scheme on graded meshes for the three-dimensional PIDEs with multi-term weakly singular kernels, *Numer. Algor.*, **2025** (2025), 1–34. https://doi.org/10.1007/s11075-025-02246-y

45. J. X. Zhang, X. H. Yang, S. Wang, A three-layer FDM for the Neumann initial-boundary value problem of 2D Kuramoto-Tsuzuki complex equation with strong nonlinear effects, *Commun. Nonlinear Sci. Numer. Simul.*, **152** (2026), 109255. https://doi.org/10.1016/j.cnsns.2025.109255

46. X. H. Yang, Z. M. Zhang, On conservative, positivity preserving, nonlinear FV scheme on distorted meshes for the multi-term nonlocal Nagumo-type equations, *Appl. Math. Lett.*, **150** (2024), 108972. https://doi.org/10.1016/j.aml.2023.108972

47. J. X. Zhang, X. H. Yang, A three-layer finite difference scheme for the nonlinear Kuramoto-Tsuzuki complex equation with variable coefficients, *Math. Methods Appl. Sci.*, **49** (2025) 108–118. https://doi.org/10.1002/mma.70138

48. Y. Shi, X. H. Yang, The pointwise error estimate of a new energy-preserving nonlinear difference method for supergeneralized viscous Burgers' equation, *Comput. Appl. Math.*, **44** (2025), 257. https://doi.org/10.1007/s40314-025-03222-x

49. Y. Shi, X. H. Yang, A time two-grid difference method for nonlinear generalized viscous Burgers' equation, *J. Math. Chem.*, **62** (2024), 1323–1356. https://doi.org/10.1007/s10910-024-01592-x

50. J. Kim, Nonlinear dynamic evolution of a novel normalized time-fractional Burgers equation, *Part. Differ. Equ. Appl. Math.*, **13** (2025), 101096. https://doi.org/10.1016/j.padiff.2025.101096

51. H. G. Lee, S. Kwak, Jyoti, Y. Nam, J. Kim, A normalized time-fractional Korteweg–de Vries equation, *Alexandria Eng. J.*, **125** (2025), 83–89. https://doi.org/10.1016/j.aej.2025.03.137

AIMS Press